Journal Pre-proof

Blue luminescent amino-functionalized graphene quantum dots as a responsive material for potential detection of metal ions and malathion

Sladjana Dorontic, Aurelio Bonasera, Michelangelo Scopelliti, Marija Mojsin, Milena Stevanovic, Olivera Markovic, Svetlana Jovanovic

PII: S0022-2313(22)00586-5

DOI: https://doi.org/10.1016/j.jlumin.2022.119311

Reference: LUMIN 119311

To appear in: *Journal of Luminescence*

Received Date: 6 April 2022

Revised Date: 12 August 2022

Accepted Date: 9 September 2022

Please cite this article as: S. Dorontic, A. Bonasera, M. Scopelliti, M. Mojsin, M. Stevanovic, O. Markovic, S. Jovanovic, Blue luminescent amino-functionalized graphene quantum dots as a responsive material for potential detection of metal ions and malathion, *Journal of Luminescence* (2022), doi: https://doi.org/10.1016/j.jlumin.2022.119311.

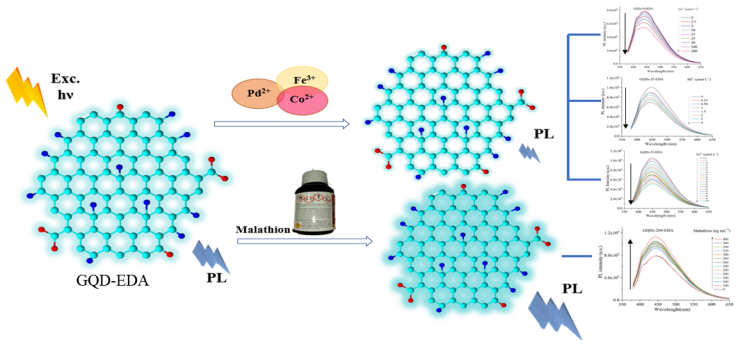

Blue luminescent amino-functionalized graphene quantum dots as a responsive material for potential detection of metal ions and Malathion

Sladjana Dorontic[a], Aurelio Bonasera[b], Michelangelo Scopelliti[b], Marija Mojsin[c], Milena Stevanovic[c,d,e], Olivera Markovic[f], Svetlana Jovanovic[*a]

[a]Vinča Institute of Nuclear Sciences-National Institute of the Republic of Serbia, University of Belgrade, P.O. Box 522, 11000 Belgrade, Serbia

[b]Dept. of Physics and Chemistry, Emilio Segrè, University of Palermo and Consorzio Interuniversitario Nazionale per la Scienza e Tecnologia dei Materiali (INSTM), Palermo Research Unit, Viale delle Scienze, bldg. 17, 90128, Palermo, Italy

[c]Institute of Molecular Genetics and Genetic Engineering, University of Belgrade, 11042 Belgrade 152, Serbia

[d]Faculty of Biology, University of Belgrade, Studentski Trg 16, 11000 Belgrade, Serbia

[e]Serbian Academy of Sciences and Arts, Knez Mihailova 35, 11000 Belgrade, Serbia

[f]University of Belgrade-Institute of Chemistry, Technology and Metallurgy, Department of Chemistry, Njegoševa 12, 11000 Belgrade, Republic of Serbia

Abstract

Large amounts of hazardous and toxic substances in the environment require non-toxic, cheap, easy, rapid, and sensitive methods for their detection. Blue luminescent graphene quantum dots (GQDs) were produced by electrochemical cleavage of graphite electrodes followed by gamma irradiation in the presence of ethylenediamine (EDA). Modified dots were able to detect metal ions (Co^{2+}, Pd^{2+}, Fe^{3+}) due to photoluminescence quenching. The highest sensitivity was detected for the sample irradiated at a dose of 25 kGy. The limits of detection (LODs) were 1.79, 2.55, and 0.66 μmol L^{-1} for Co^{2+}, Fe^{3+}, and Pd^{2+}, respectively. It was observed that GQDs irradiated at 200 kGy act as an ultra-sensitive turn-on probe for Malathion detection with LOD of 94 nmol L^{-1}. Atomic force microscopy images proved the aggregation of GQDs in the presence of the investigated metal ions. Results obtained by 3-(4,5-dimethylthiazol-2-yl)-2,5-diphenyltetrazolium bromide (MTT) assay and LIVE/DEAD

[*]Corresponding author: S. Jovanovic, email: svetlanajovanovic@vin.bg.ac.rs; P.O. Box 522, 11000 Belgrade, Serbia

cytotoxicity test indicated that GQDs irradiated with EDA are not toxic towards MRC-5 cells, which makes them a promising, eco-friendly and safe material for sensing application.

Keywords: amino-functionalized graphene quantum dots; gamma irradiation; photoluminescence; probe; metal ions; malathion.

1. Introduction

Human population growth and urbanization have led to the intensive development of agriculture, mining, food, car, and pharmaceutical industry. Due to wrong handling or improper disposal, many toxic and hazardous substances find their way to natural media, finally compromising the biosphere equilibrium. The most common pollutants are metal ions and pesticides [1, 2]. Although Fe^{3+} and Co^{2+} ions are involved in metabolic processes [3], their high concentrations may lead to cell membrane damage, destabilization of proteins, and cardiotoxicity [4, 5]. Noble metals such as palladium are widely used in organic chemistry, the pharmaceutical industry, and medicine due to their outstanding catalytic and anti-cancer activity. Nevertheless, long-term exposure leads to serious health issues [6]. Apart from metal ions, pesticides are the most toxic agents in the environment. Some of them are blocking the enzyme's activity, such as malathion inhibiting acetylcholinesterase [7]. It is a wide-spectrum organophosphate insecticide with reported toxic effects on the liver, kidney, testis, ovaries, lung, pancreas, and blood [8]. Because of this, monitoring the presence and the concentration of both pesticides and metal ions in the water, air, soil, food, and biological samples is of priority importance [9].

Since their discovery, graphene quantum dots (GQDs) have become a rising star in modern material science [10]. GQDs are zero-dimensional carbon-based nanomaterials. Their graphene-like core is composed of sp^2-hybridized C atoms which are organized according to a hexagonal honeycomb crystal lattice, with oxygen functional groups (epoxy, hydroxy, carboxy, and carbonyl) attached to the surface and at the edges [11]. Thanks to their intense photoluminescence (PL) in the visible part of the spectrum, high absorption of ultraviolet light, impressing photostability, resistance to photobleaching, non-toxicity, and biocompatibility, they are widely investigated for bioimaging and sensing applications [12]. The origin of PL GQDs has not been ascertained yet, but significant contributors are quantum-confinement effect, edge effect (zig-zag or armchair edge), functional groups or heteroatoms attached on the surface, radiative recombination of electron-hole pairs, and vacancy defects [11, 13]. By setting synthetic conditions or by post-synthesis treatments and

functionalization, morphological, structural, and optical properties of GQDs can be finely tuned [11, 13-17]. Surface doping can increase the PL intensity, which is an important parameter for optical detection but also generates additional sites for the binding of the analytes. In presence of some ions and organic molecules like pesticides, the PL intensity of GQDs may decrease or increase, leading to two detection mechanisms: turn-off and turn-on pathways [9]. Changes in PL intensity are explained by different interactions between GQDs and analytes such as metal-ligand interactions and electron transfer in case of a turn-off, and the establishment of hydrogen bonds between GQDs functional groups and analytes in the case of a turn-on mechanism [18-20]. It was confirmed that these interactions caused aggregation of GQDs [18, 20].

GQDs were examined as PL probes for different pollutants. Ma et al. investigated amino acid-functionalized GQDs as a PL probe for Fe^{3+} detection in an aqueous medium [3]. It was observed that with an increase in Fe^{3+} concentration, the PL intensity of GQDs was quenched. The limit of detection (LOD) was 50 nmol L^{-1}. Co^{2+} ions were detected by Boonta et al. using N, S co-doped GQDs [5]. LOD was 1.25 μmol L^{-1}. A study pointing at the detection of Pd^{2+} ions using GQDs as a sensing platform wasn't found in the literature, but carbon nanoparticles (CNPs) were examined by Sharma et al. [21]. A linear response was found in the range of 35-100 μmol L^{-1}, with a LOD of 58 n mol L^{-1}. Malathion was detected by Roushani et al. using GQDs as a dual turn-off/turn-on probe for both Hg^{2+} and malathion [22]. Obtained LOD for malathion was 0.5 μmol L^{-1}.

In previous research, we successfully introduced amino groups in the structure of GQDs, using gamma irradiation at doses of 25, 50, and 200 kGy, respectively, with ethylenediamine (EDA) as a nitrogen source [23], and achieved the increase of PL quantum yield from 2.07 to 18.40%. In this paper, we studied gamma-irradiated, amino-functionalized GQDs as an optical platform for the detection of Co^{2+}, Pd^{2+}, and Fe^{3+} ions, and the insecticide malathion. A PL intensity of all GQDs in the presence of these analytes was measured using PL spectroscopy. Linearity of PL change in dependence of analyte concentration was determined using the Stern-Volmer equation and LODs were calculated. Morphological properties of GQDs in presence of Co^{2+}, $Pd^{2+,}$ and Fe^{3+} ions were studied using atomic force microscopy (AFM) and the aggregation was described. Also, we tested the biological effects of gamma-irradiated GQDs on MRC-5 cells using (3-(4,5-dimethylthiazol-2-yl)-2,5-diphenyltetrazolium bromide) (MTT) cytotoxicity assay and LIVE/DEAD test.

2. Experimental

2.1. Chemicals and materials

Graphite electrodes (99.999 % purity, ø = 3.05 mm) were purchased from Ringsdorff-Werke GmbH (Bonn, Germany). Ethanol (96 vol%), sodium hydroxide, isopropyl alcohol (IPA), acetone, and hydrochloride acid (37 vol%) were purchased from Fisher Scientific (Loughborough, Leicestershire, UK), dialysis bags (MCWO 3.5 kDa) from Spectrum Laboratory Inc. (San Pedro St., Gardena, CA, USA), ethylenediamine (EDA) (≥ 99.5 %) from Carl Roth GmbH (Schoemperlenstr, Karlsruhe, Germany). Cobalt (II) chloride hexahydrate ($CoCl_2 \times 6\ H_2O$) and iron (III) nitrate-nonahydrate ($Fe\ (NO_3)_3 \cdot 9\ H_2O$) were purchased from VWR Chemicals (Geldenaaksebaan, Leuven, Belgium). Palladium (II) chloride ($PdCl_2$) was purchased from Termofisher (Kandel) GmbH (Zeppelinstrasse, Karlsruhe, Germany). Etiol® (malathion- (Diethyl (2S)-2-[(dimethoxyphosphorothioyl)sulfanyl]succinate), min. 95 %, Galenika a.d. Belgrade, Serbia was bought in a local agricultural pharmacy. LIVE/DEAD™ Cell Imaging Kit was purchased from Invitrogen (Paris, France). Penicillin and streptomycin were purchased from Sigma Aldrich (Merck, KGaA, Darmstadt, Germany).

2.2. Synthesis of graphene quantum dots

GQDs were synthesized by the previously described electrochemical approach using graphite electrodes as a starting material [23]. First, graphite electrodes were washed in ultrapure water and ethanol. Then, 3g of NaOH were dispersed in 100 ml of 96 vol% ethanol. The dispersion was sonicated for 6 h. Graphite electrodes were used as cathode and anode and immersed in NaOH dispersion. The current was set at 20 mA and the potential was 20 mV. After 24 h, dispersion changed color from orange to dark brown. To obtain pure GQDs, ethanol was first evaporated to return dry powder. NaOH was removed using dialysis. The pH value was monitored until it reached 7. This sample was labeled as p-GQDs. Amino-functionalized GQDs were prepared by gamma irradiation of p-GQDs at three different doses and in the presence of EDA. Water dispersion of p-GQDs in the concentration of 1 mg mL^{-1} was mixed with isopropyl alcohol (IPA) (3 vol% in total) and sonicated for 10 min. After, EDA was added in 4 vol% in total. Samples were sonicated for 15 min and purged with Ar. These mixtures were irradiated at doses of 25, 50, and 200 kGy. As a source of gamma irradiation, a Co-60 was used. After irradiation, samples were dialyzed to remove the

irradiation medium. Samples of GQDs irradiated with 25, 50, and 200 kGy were labeled as GQD-25-EDA, GQD-50-EDA, and GQD-200-EDA, respectively.

2.3. Characterization of graphene quantum dots

2.3.1. Atomic force microscopy (AFM)

Morphological properties of GQDs were analyzed using atomic force microscopy (AFM). Prepared samples were spin-coated on mica (3500 rpm, 1min) and recorded using Quesant (Agoura Hills, CA, USA) AFM which was operating in the tapping mode, in the air, at room temperature. Standard silicon tip (NanoAndMore Gmbh, Wetzlar, Germany) was used with the constant force of 40 N m^{-1}. Q-WM300 AFM probe rotated, monolithic silicone probe for non-contact high-frequency application was used. To examine the morphological properties of GQDs in the presence of metal ions, GQDs-50-EDA were mixed with Co^{2+} and Pd^{2+}, separately and GQDs-25-EDA were mixed with Fe^{3+} in ultrapure water. Concentrations of GQDs and ions in all samples were 0.28 mg mL^{-1} and 200 µmol L^{-1}, respectively. AFM images were analyzed using Gwyddion 2.58 software [24].

2.3.2. Transmission electron microscope (TEM)

JEOL JEM-2100F transmission electron microscope (TEM) was employed to investigate the morphology of GQDs. Water dispersions of dots were prepared in a concentration of 1 mg mL^{-1}. As support, carbon laced copper grids were selected. To measure the diameter of GQDs, ImageJ software was used.

2.3.3. X-ray photoelectron spectroscopy (XPS)

The XPS spectra of modified GQDs were obtained using ULVAC-PHI500 VersaProbe II scanning microprobe (ULVAC-PHI, Inc., Chigasaki, Japan) with an Al Kα source (1486.6 eV), 100 µm spot, 25W, 15 kV. The sample was deposed on a surface kept at 45° with respect to the analyzer, working in FAT mode. All spectra were recorded using a dual neutralization system (both e^- and Ar^+). All binding energy (BE) values are referenced to C 1s hydrocarbon peak at 284.8 eV.

2.3.4. EA

Samples of GQDs were dried under reduced pressure and powder samples were used for measurement. Elemental analysis was performed on a Vario EL III C,H,N,S/O Elemental Analyzer (Elementar GmbH, Germany).

2.3.5. UV-Vis spectroscopy

Absorption spectra of GQDs-25-EDA in the presence of Co^{2+}, Pd^{2+}, and Fe^{3+} were obtained using LLG-uniSPEC 2 Spectrophotometer (Lab Logistic Group, Meckenheim, Germany) in the wavelength range of 200-800 nm, at room temperature. The concentration of GQDs in all samples was 0.03 mg mL^{-1}, while the concentrations of the metal ions were 0, 25, 50, 100, and 200 μmol L^{-1}. All spectra were recorded in ultrapure water.

2.3.6. Photoluminescent (PL) spectroscopy

To examine photoluminescent properties, GQDs-25-EDA, GQDs-50- EDA, and GQDs-200-EDA were dispersed in ultrapure water, at different concentrations (from 0.040 to 0.300 mg mL^{-1}) and concentration of 0.125 mg mL^{-1} was selected as optimal and used in studies of PL properties of GQDs. PL spectra were recorded on the Horiba Jobin Yvon Fluoromax-4 spectrometer (Horiba, Kyoto, Japan) under different excitation wavelengths (300, 320, 340, 360, 380, and 400 nm) in the wavelength range of 320-580 nm. Excitation and emission slits were 8 and 2 nm, respectively. Integration time was 0.5 s. All spectra were recorded at room temperature and atmospheric pressure. Photoluminescent quantum yields (PL QY) were calculated using the equation below [25]:

$$QY_{GQDs}=QY_{REF}(A_{REF}/A_{GQDs})(F_{GQDs}/F_{REF})(n_{GQDs}/n_{REF})^2$$

where *QY* is photoluminescent quantum yield of GQS samples, *F* is integrated intensity of emission band, *A* is the value of the absorbance, *n* is the refractive index of the solvent, while subscripts 'REF' refers to reference, Rhodamine B with known PL QY=31% [25, 26]. For these measurements, diluted dispersion of GQDs were used, at a concentration of 0.04 mg mL^{-1}, in water.

The stability of PL intensity was examined under the different experimental conditions. GQDs-25-EDA were exposed to UV lamp (300 nm) in different time intervals: 0, 15, 30, 60, 120, 180, and 480 min, and at different pH values: 1,3,5,7,8,10, and 12. pH values were set using NaOH and HCl. All spectra were recorded at 360 nm excitation wavelength.

2.4. Detection of Co^{2+}, Pd^{2+}, Fe^{3+}, and malathion

2.4.1. Sample preparation

For Co^{2+} and Pd^{2+} detection, a series of concentrations from 0 to 200 μmol L^{-1} were made. Also, the detection of Pd^{2+} ions was investigated in the concentration range 0-4 μmol L^{-1}. Fe^{3+} was tested in the range of 0-100 μmol L^{-1}. The concentration of gamma-irradiated GQDs in all samples was 0.03 mg mL^{-1}. Mixtures were incubated for 2 min at room temperature before measurement. Malathion in concentrations from 0 to 400 ng mL^{-1} was mixed with gamma-irradiated GQDs dispersion in ethanol, in the concentration of 0.03 mg mL^{-1}. Samples were incubated 24 h before measurement, to establish interaction between GQDs and the insecticide molecule.

2.4.2. Photoluminescence measurement

PL spectra of GQDs-25-EDA, GQDs-50-EDA, and GQDs-200-EDA in the presence of Co^{2+}, Pd^{2+}, Fe^{3+}, and malathion were obtained using Horiba Jobin Yvon Fluoromax-4 spectrometer at room temperature under 360 nm excitation wavelength. Integration time was 0.5 s. Selectivity of GQDs-25-EDA toward Co^{2+}, Pd^{2+} and Fe^{3+} ions. To evaluate a specifical recognition ability of GQDs-25-EDA to Co^{2+}, Pd^{2+} and Fe^{3+} ions, the PL intensity in the presence of these ions were compared with intensities in the presence of the Na^{+}, K^{+}, Ca^{2+}, Fe^{2+}, Cu^{2+}, Ni^{2+}, Zn^{2+}, and Ag^{+} as well as in the mixture of these ions.

2.4.3. Detection of Co^{2+}, Pd^{2+} and Fe^{3+} in the real samples: river and tap water

To evaluate the practical applicability of GQDs-25-EDA as a PL probe for Co^{2+}, Pd^{2+}, and Fe^{3+} in the real samples, tap and water from the river were chosen. Tap water was used without any purification. The river water was centrifugated at 3500 rpm, for 1h, and filtrated to eliminate solid impurities. Samples were prepared with different concentrations of ions solutions (0, 25, 50, 75, and 100 μmol L^{-1}). All spectra were recorded at 360 nm excitation wavelength. Recovery tests (R%) are performed by measuring the PL intensity of water

samples in which Co^{2+}, Pd^{2+}, and Fe^{3+} in the concentration of 75 μmol L^{-1} were spiked into the samples. The concentrations of ions were calculated from calibration curves.

2.5. Cytotoxicity investigation

To examine cell viability in presence of investigated GQDs, an MTT cytotoxicity assay and LIVE/DEAD cytotoxicity test were used. MRC-5 cells (fibroblasts derived from normal lung tissue) were grown in Dulbecco's Modified Eagle's Medium (DMEM) supplemented with 10 % fetal bovine serum and penicillin/streptomycin (10.000 units penicillin and 10 mg streptomycin mL^{-1}) at 37 ^{o}C in a humidified atmosphere with 5 % CO_2.

2.5.1. MTT cytotoxicity assay

For the MTT assay, MRC-5 cells were seeded in a 96-well plate ($2x10^4$ cell $well^{-1}$) and allowed to adhere to the plate overnight. After 24 h, cells were treated with increasing concentrations (1, 10, 25, 50, and 100 μg mL^{-1}) of p-GQD, GQD-25-EDA, GQD-50-EDA, and GQD-200-EDA during 24, 48, and 72 h. Following treatments cell viability was determined using an MTT assay (Merk KGaA, Darmstadt, Germany). Absorbance was measured at 540 nm using Tecan Infinite 200 Pro multiplate reader (Tecan Group, Mannedorf, Switzerland). All experiments were repeated at least three times. The relative viability (%) of cells treated with methanol, as vehicle control, was set to 100 %.

2.5.2. LIVE/DEAD cytotoxicity test

For the LIVE/DEAD cytotoxicity test, water dispersions of p-GQDs, GQDs-25-EDA, GQDs-50-EDA, and GQDs-200-EDA in the concentration of 3 mg mL^{-1} were prepared. MRC-5 cells were seeded on coverslips in 12 well plates in concentration 5×10^4 cells/well. After 24 h, 100 μg mL^{-1} of p-GQDs, GQD-25-EDA, GQD-50-EDA, and GQD-200-EDA were added to the cells and further incubated for 48h. Cytotoxicity was measured by a two-color discrimination system of live (green fluorescence) and dead (red fluorescence) cells using the LIVE/DEAD™ Cell Imaging Kit. Cells were visualized using Olympus BX51 fluorescence microscope, FITC filter for green fluorescence, and Cy5 for red fluorescence, and analyzed using Cytovision 3.1. software (Applied Imaging Corporation, USA). All images were captured at 20x objective.

3. Results and discussion

3.1. Analysis of morphology, structure, and optical properties of GQDs

Morphological properties of GQDs were investigated by AFM and TEM. In Figure 1 AFM images of GQDs-25-EDA (a), GQDs-50-EDA (b), and GQDs-200-EDA (c) with their height profiles are presented. GQDs irradiated with 25 and 50 kGy are uniformly distributed spherical nanoparticles with a height in the range of 0.5-2 nm, which corresponds to 1-4 graphene layers [23]. On the contrary, GQDs irradiated with the dose of 200 kGy exhibits a height up to 20 nm and form agglomerates. TEM images of GQD-25-EDA and GQDs-50-EDA showed that the lateral sizes of dots were below 20 nm, while in the case of GQD-200-EDA the diameter was above 30 nm.

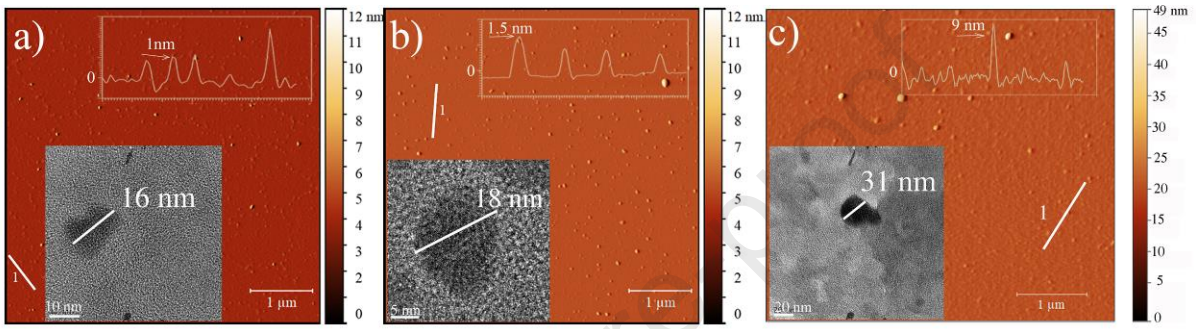

Figure 1. AFM images with height profiles and TEM micrographs in the lower left corner of GQDs-25-EDA (a), GQDs-50-EDA (b), and GQDs-200-EDA (c).

Structural analysis of gamma-irradiated GQDs was conducted by means of XPS. Surveys scans of GQDs-25-EDA (a), GQDs-50-EDA (b), and GQDs-200-EDA (c), in the energy range of 1100-0 eV, 1.0 eV resolution, are shown in Fig. 2. All samples show the expected characteristic strong peaks of C 1s (≈ 285 eV) and O 1s (≈ 532 eV). All samples also show a smaller peak, at 400 eV, in the range of N 1s, indicative of the incorporation of nitrogen atoms in the GQD structure.

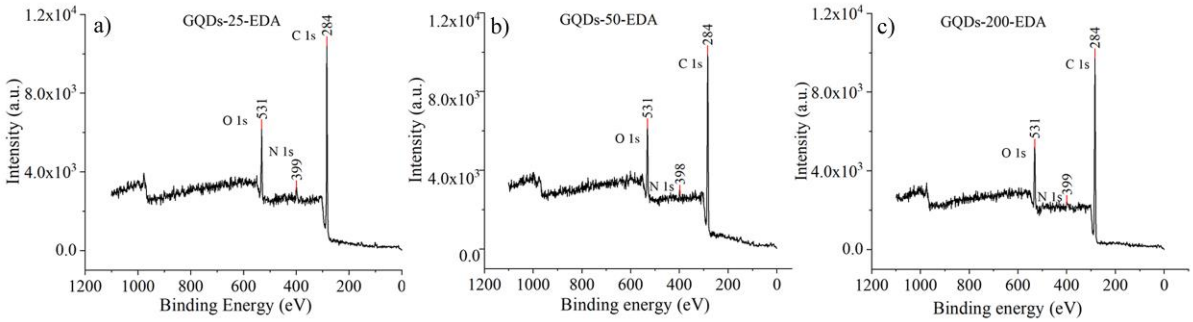

Figure 2. XPS survey scan of GQDs-25-EDA (a), GQDs-50-EDA (b), and GQDs-200-EDA (c). Resolution 1.0 eV.

Deconvoluted C 1s spectra of GQDs-25-EDA, GQDs-50-EDA, and GQDs-200-EDA are presented in the previous study [18]. Analyzed spectra of the O 1s region are shown in Fig. 3. GQDs-25-EDA (a), GQDs-50-EDA (b), and GQDs-200-EDA (c) all show the presence of a single species, centered at 531.9 eV, 532.2 eV, and 532.0 eV respectively. All values are compatible with the carbonyl functional group [27-30].

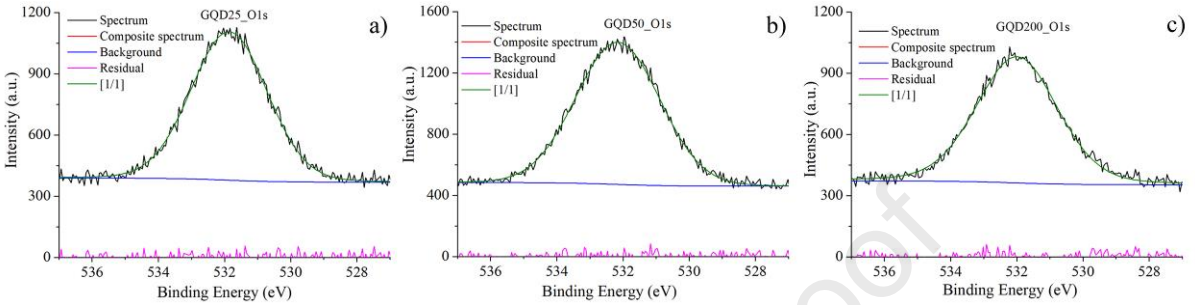

Figure 3. Analysis of O 1s region for GQDs-25-EDA (a), GQDs-50-EDA (b), and GQDs-200-EDA (c).

In the N 1s XPS spectra of γ-irradiated GQDs, all samples show a single species, attributable to amine nitrogen [31]. Found values are 399.4 eV, 399.8 eV, and 399.5 eV for GQDs-25-EDA, GQDs-50-EDA, and GQDs-200-EDA, respectively – see Figure 4. In the N 1s XPS spectra of gamma-irradiated GQDs, peaks at 399.4 (Figure 4a), 399.8 (Figure 4b), and 399.5 eV (Figure 4c) indicated a presence of N-H/N-C bonds in the amino group.

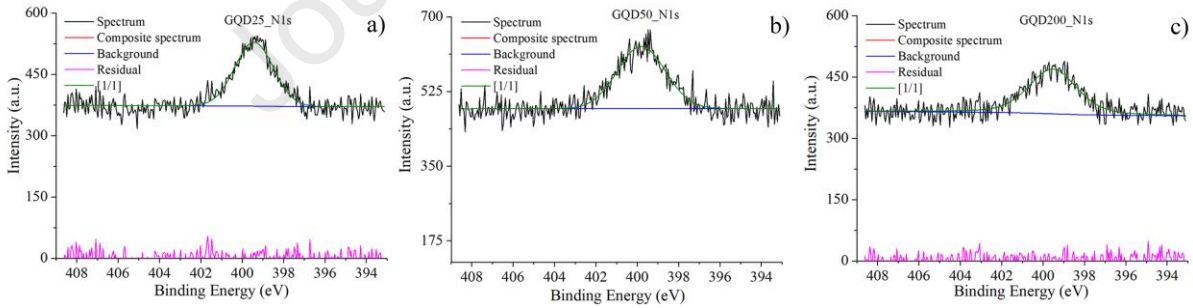

Figure 4. Analysis of N 1s region spectra for GQDs-25-EDA (a), GQDs-50-EDA (b), and GQDs-200-EDA (c).

Presented results indicated that after gamma irradiation, GQDs had C=O and C-NH_2 functional groups. It was observed that UV irradiation lead to free radical polymerization of salicylic acid and 2,6-Pyridinedicarboxylic acid and highly luminescent N-doped GQDs were produced [32]. On the opposite, gamma irradiation belongs to high-energy short wavelengths of electromagnetic waves that are able to induce ionization. Gamma rays lead to radiolytic

decomposition of all molecules in the system, as presented in reactions 1-4. When anhydrous EDA was exposed to gamma rays, the production of gasses (hydrogen, methane, ethylene, ammonia), volatile liquid, and polymerized products were observed [33]. With dose, the content of the hydrogen and methane was increased. When oxygen is present in the dilute aqueous EDA solution the main radiolytic product is ammonia due to OH radicals that were primarily involved in decomposition [34]. It was reported that graphene oxide (GO) can be reduced by gamma irradiation in a mixture of alcohol and water [35]. When oxygen was removed from the system, and alcohol such as IPA was added, OH radicals formed in the radiolytic decomposition of H_2O were quenched with IPA [23, 36, 37]. Thus, the main species are reductive once, such as hydrogen radicals and hydrated electrons, as well as those solvated electrons produced from irradiated ethylenediamine [38]. A previous study suggested that EDA molecules react with both oxidative ($^{\bullet}OH$) and reductive ($^{\bullet}H$) species [39]. In the proposed system following reactions were occurred:

Reaction 1: H_2O + gamma rays → $^{\bullet}H + HO^{\bullet} + e_{aq} + HOO^{\bullet} + HO^{-} + H_3O^{+} + H_2 + H_2O_2$ [40]

Reaction 2: H_2O + IPA + gamma rays → $^{\bullet}H + e_{aq} + HO^{-} + H_3O^{+} + H_2 + (CH3)_2\dot{C}HOH$ [41]

Reaction 3: $NH_2CH_2CH_2NH_2 + {}^{\bullet}OH/{}^{\bullet}H \rightarrow NH_2\dot{C}HCH_2NH_2 + H_2O/H_2HNH_2 + H_2O/H_2$ [42, 43]

Reaction 4: $NH_2CH_2CH_2NH_2 + {}^{\bullet}OH/{}^{\bullet}H \rightarrow NH_2CH_2CH_2\dot{N}H + H_2O/H_2$ [43]

Thus, in our experiment, the following radicals were produced

Reaction 5: $H_2O + IPA + NH_2CH_2CH_2NH_2$ + gamma rays → $^{\bullet}H, + e_{aq} + H_2HNH_2 + H_2 + (CH3)_2\dot{C}HOH + NH_2\dot{C}HCH_2NH_2 + NH_2CH_2CH_2\dot{N}H$

While reductive species ($^{\bullet}H$, e_{aq}) induce the reduction of oxygen-containing functional groups on GQDs surface, such as carbonyl into OH, with epoxy into OH, with OH groups into H2O and restored C=C bonds or EDA radical might react with carbonyl groups leading to amide bond formation [43].

Apart from the indirect effects of gamma irradiation on GQDs that occur through decomposition of the irradiation medium, there is also a direct effect of gamma rays on carbon nanostructures [37]. High-energy gamma photons are able to knock out C atoms from graphene sheets creating holes [44], cutting [45], or interlayer bonds [46].

Furthermore, table 1 shows the elemental analysis results of p-GQDs, GQD-25-EDA, and GQDs-50-EDA. For p-GQDs, N atoms were not detected, while after irradiation in the presence of EDA, 7.42 and 6.81 wt.% of N was detected. The changes in C content were observed as well. The wt.% of C was increased by 8.92 % at a dose of 25 kGy, while at 50 kGy C was increased by 10.15 %. Thus, gamma irradiation with EDA leads to incorporation of N atoms in GQDs structure and to chemical reduction due to an increase in C content which is in agreement suggested mechanism of reduction with $^{\bullet}H$ and e_{aq} as well as previous measurements [23].

Table 1. Elementar analysis of p-GQDs, GQDs-25-EDA, and GQDs-50-EDA.

Sample	**N** (wt.%)	**C** (wt.%)	**H** (wt.%)	**S** (wt.%)
p-GQDs	/	44.32	5.27	/
GQDs-25-EDA	7.42	53.24	7.14	/
GQDs-50-EDA	6.81	54.47	7.21	/

In Figure 5 emission spectra of GQDs-25-EDA (a), GQDs-50-EDA (b), and GQDs-200-EDA (c), respectively, are presented. A PL intensity was measured under different wavelengths of excitation light in the range of 300-400 nm. With excitation wavelengths change, emission peaks positions in all three samples were changed. Maximums of emission peaks were shifted from 435, 451, and 435 nm (λ_{exc}= 300 nm) to 465, 467, and 466 nm (λ_{exc}= 400 nm), for GQDs-25-EDA, GQDs-50-EDA, and GQDs-200-EDA, respectively. This behavior of GQDs in literature was reported as excitation-depended photoluminescence [47]. It is assumed that the position of emission band dependence of excitation light wavelengths originates from edge state, emissive traps, electron-conjugated systems, heteroatoms, and functional groups attached on GQDs surface, quantum size effect, etc. [48]. The shift in emission band was observed when GQDs were doped with N atoms in different %, from 5.5 to 2.4, from blue to orange [49]. Herein, N was incorporated in the form of graphitic N. Another study showed that when the% of N dopant is increased, the emission band was shifted towards lower wavelengths [32].

Relative values of PL quantum yields (PL QY) are calculated for an excitation wavelength of 360 nm and obtained values were 5.82, 1.89, and 28.01 % for GQDs-25-EDA, GQDs-50-EDA, and GQDs-200-EDA, respectively.

From the PL spectra can be observed that all three kinds of amino-doped GQDs possess maximums of PL intensity in the blue region of the spectrum. For comparison, if we refer to p-GQDs emission spectra presented in previous work [23], it can be seen that the excitation dependence is more pronounced in pristine samples than in GQDs-EDA, under the same excitation wavelengths. Shift of emission peak in p-GQDs was from 430 nm (λ_{exc}= 300 nm) to 495 (λ_{exc}= 400 nm) [23]. It can be explained by greater stability of surface state and uniformity of size distribution in GQDs-EDA than in p-GQDs. Thus, the functionalization with amino groups in gamma irradiation conditions affects GQD's optical properties.

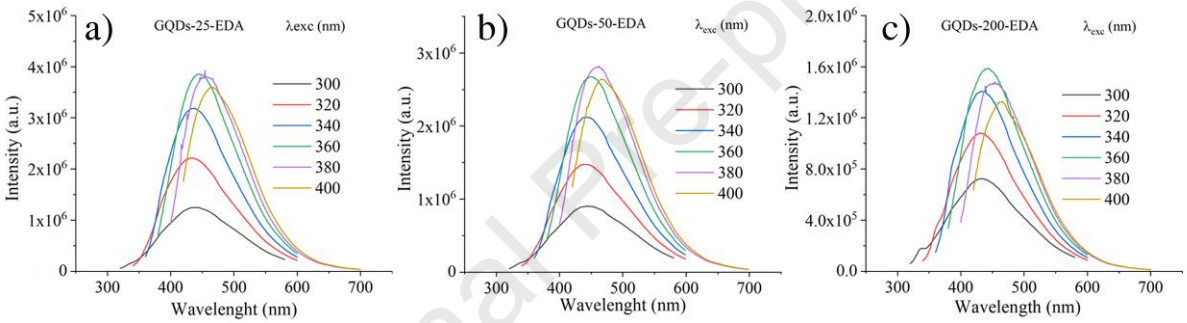

Figure 5. PL emission spectra of GQDs-25-EDA (a), GQDs-50-EDA (b), and GQDs-200-EDA (c) under excitation wavelengths from 300 to 400 nm.

In Figure 6a, the relative PL intensities obtained after GQDs-25-EDA were exposition to continuous UV irradiation (wavelength of 300 nm) in different time intervals of 0, 15, 30, 60, 120, 180, and 480 min are presented. The “I” is the PL intensity after irradiation, while the “I_0” is the value of PL intensity measured before irradiation. The PL intensities showed no significant changes after 480 min of UV irradiation. The effect of pH on the PL intensity of GQDs-25-EDA in a range of 1-12 was studied (Figure 6b). PL intensity of GQDs was relatively stable in the pH range of 2-8, reaching a maximum at pH 10, while when pH was 1 and 10 show a large change (Figure 6b.) Obtained results indicate that the PL intensity of the GQDs-25-EDA exhibits good stability when they were exposed to UV irradiation and in the pH range of 2-8.

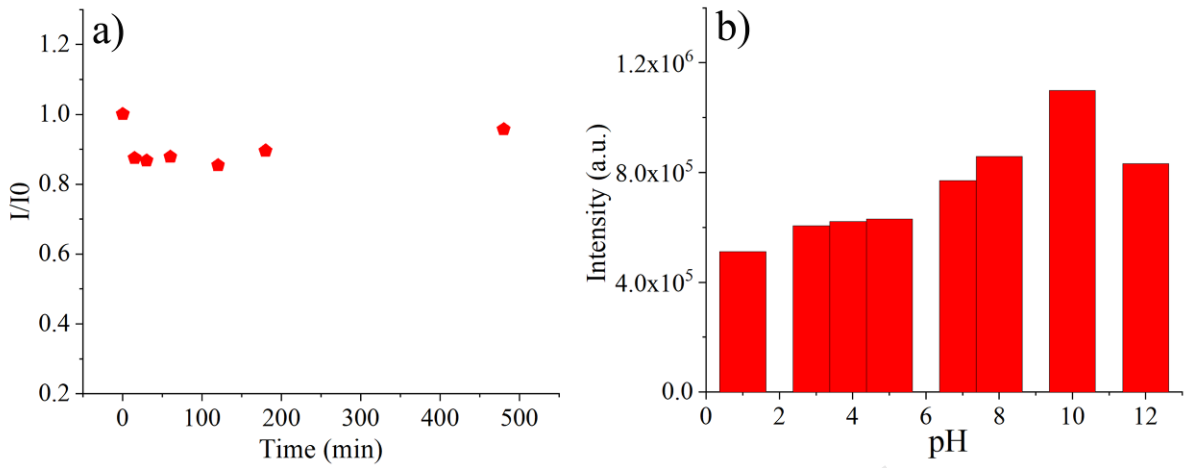

Figure 6. Values of relative PL intensities of GQDs-25-EDA after irradiation for 0 to 480 min (a), the values of PL intensities at different pH values at the excitation wavelength of 360 nm (b).

3.2. Detection of metal ions

3.2.1. Photoluminescence detection

PL spectra of GQDs-25-EDA (a), GQDs-50-EDA (b), and GQDs-200-EDA (c) under excitation wavelength of 360 nm in the presence of Co^{2+} ions at a concentration from 0 to 200 μmol L^{-1} are reported in Figure 7. In PL spectra, a significant decrease in emission band intensity was detected when the Co^{2+} concentration was increased. The quenching efficiencies of GQD probes were calculated according to the general Stern-Volmer equation: $A_0/A = 1 + Ksv [Q]$ [50], where A_0 and A correspond to integrated areas under the PL intensity curve in the absence and the presence of quencher, respectively. K_{sv} is the quenching constant that corresponds to the slope obtained from linear data fitting. Linear relationship is described as $A_0/A = 1.0125 + 0.0088 [Co^{2+}]$, $A_0/A = 0.99501 + 0.0060 [Co^{2+}]$, $A_0/A = 0.9819 + 0.0074 [Co^{2+}]$, for GQDs-25-EDA, GQDs-50-EDA and GQDs-200-EDA, respectively. Figures 7d, 7e, and 7f show dependence A_0/A from Co^{2+} concentration in GQDs-25-EDA, GQDs-50-EDA, and GQDs-200-EDA, respectively, while in the lower right corners of e) and f) results of linear fitting for GQDs-50-EDA, and GQDs-200-EDA are shown. In the case of GQDs-25-EDA, a good linear response is observed in the concentration range 0-10 μmol L^{-1}, while for GQDs-50-EDA in the range 0-15 μmol L^{-1} and GQDs-200-EDA data showed a satisfying linear fitting in the range 2.5-15 μmol L^{-1}. Determination coefficient values were 0.91, 0.98 and 0.98 for GQDs-25-EDA, GQDs-50-EDA, and GQDs-200-EDA, respectively. LODs were calculated using the equation: $LOD = 3S_D/K_{sv}$, where S_D represents the standard deviation of

intercept [27]. Obtained LODs were 3.73, 2.79, and 3.71 μmol L^{-1} for GQDs-25-EDA, GQDs-50-EDA, and GQDs-200-EDA, respectively.

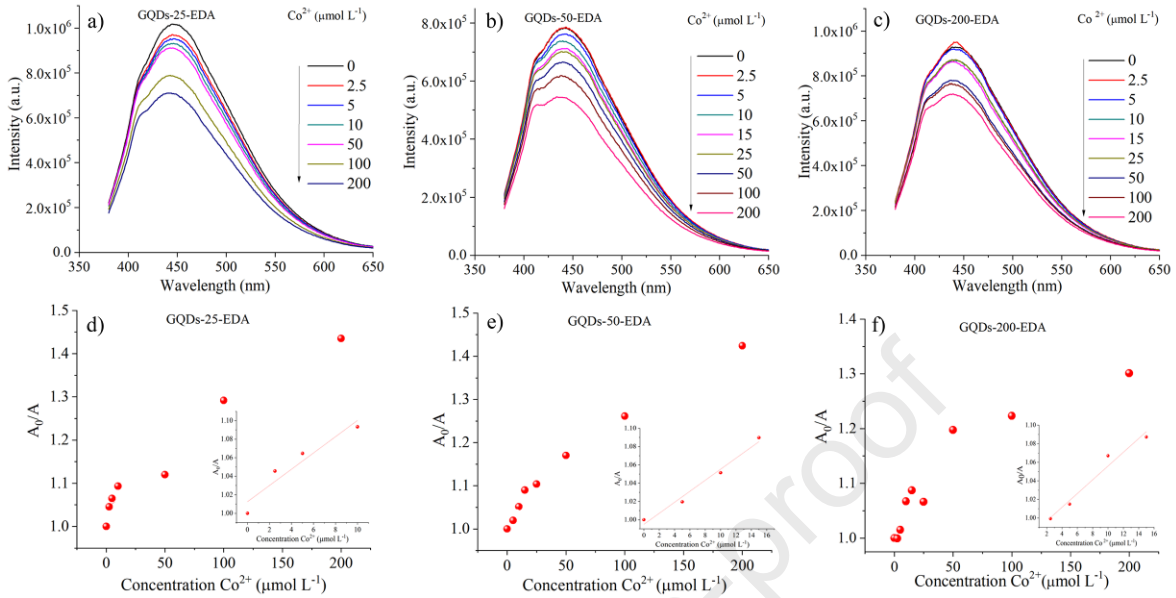

Figure 7. Emission spectra of the GQD-25-EDA (a), GQDs-50-EDA (b), and GQDs-200-EDA (c), recorded under λ_{exc}=360 nm in the presence of Co^{2+} ions in the concentration range 0-200 μmol L^{-1}. The Stern-Volmer plots (integrated area under emission peak versus concentration of Co^{2+}) for GQD-25-EDA (d), GQDs-50-EDA (e), GQDs-200-EDA (f), with a linear fitting curve for GQDs-25-EDA, GQDs-50-EDA, and GQDs-200-EDA in the upper right corner.

The samples of GQDs also were examined as a PL probe for Pd^{2+} ions. PL spectra of irradiated GQDs recorded in presence of Pd^{2+} ions in the concentration range 0-200 μmol L^{-1} show the lowering in PL intensities for all examined samples (Figures 8a, b, and c). The linear response was found in the range 0-5 μmol L^{-1} in the case of GQDs-25-EDA and GQDs-50-EDA, while for GQDs-200-EDA the linearity was in the range 5-25 μmol L^{-1}.

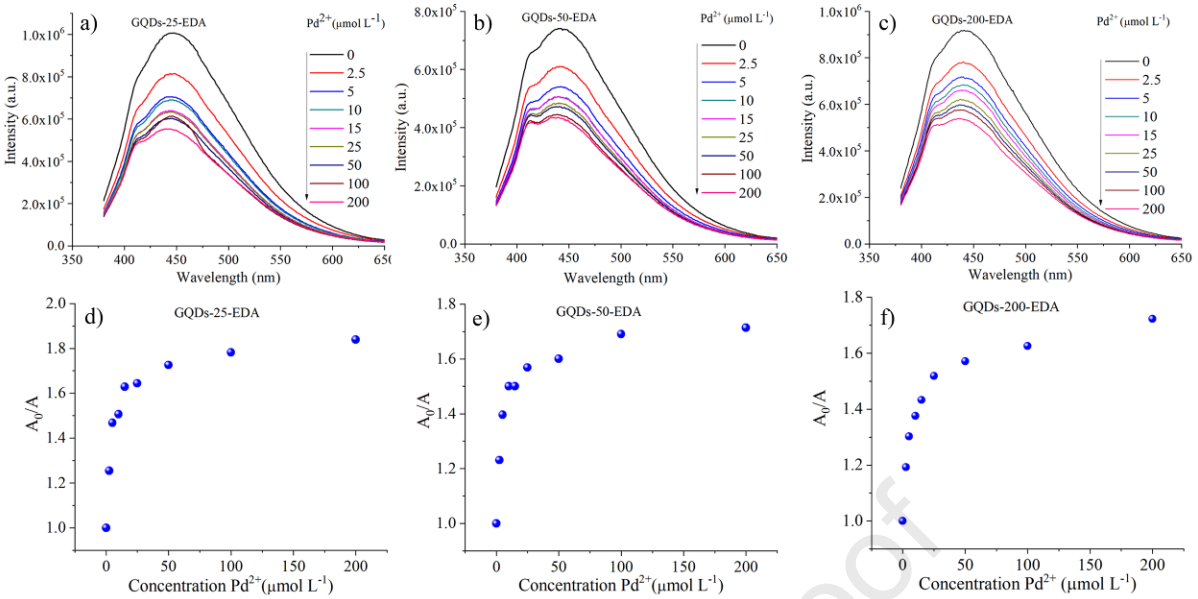

Figure 8. Emission spectra of the GQD-25-EDA (a), GQDs-50-EDA (b), and GQDs-200-EDA (c) were recorded under λ_{exc}=360 nm, in the presence of Pd^{2+} ions in the concentration range 0-200 μmol L^{-1}, and the Stern-Volmer plot (integrated area under emission peak versus concentration of Pd^{2+}) GQD-25-EDA (d), GQDs-50-EDA (e), and GQDs-200-EDA (f).

The effect of low Co^{2+} concentrations on PL intensity of GQDs is presented in Figure 9a, while the result of linear fitting in the concentration range 0-7.5 μmol L^{-1} is displayed in figure 9b. Linear relationship is defined as $A_0/A = 0.9113 + 0.0131 [Co^{2+}]$ and LOD was 1.79 μmol L^{-1} (R^2=0.911). It is observed that PL intensities decreased sharply at the Pd^{2+} lowest tested concentration. A linear response was revealed in a narrow concentration range, up to 5 μmol L^{-1}. Herein, the saturation of GQDs with analytes was observed. Based on these results, PL in presence of Pd^{2+} in the concentration range of 0-4 μmol L^{-1} (Figure 9c) was examined. Linear decrease of PL intensity was observed from 0.25 to 4 μmol L^{-1} (Figure 8d) with R^2 = 0.950. Linear relationship is described as $A_0/A = 1.1171 + 0.0093 [Pd^{2+}]$. LOD was 0.66 μmol L^{-1} which is lower than 5-10 ppm (28-56 μmol L^{-1}), a concentration range of Pd^{2+} in pharmaceutical products accepted by the World Health Organization (WHO). This value indicates the high sensitivity of investigated material [51]. According to obtained results, it can be concluded that gamma-irradiated GQDs can be used for Pd^{2+} detection in the concentration range 0-4 μmol L^{-1}.

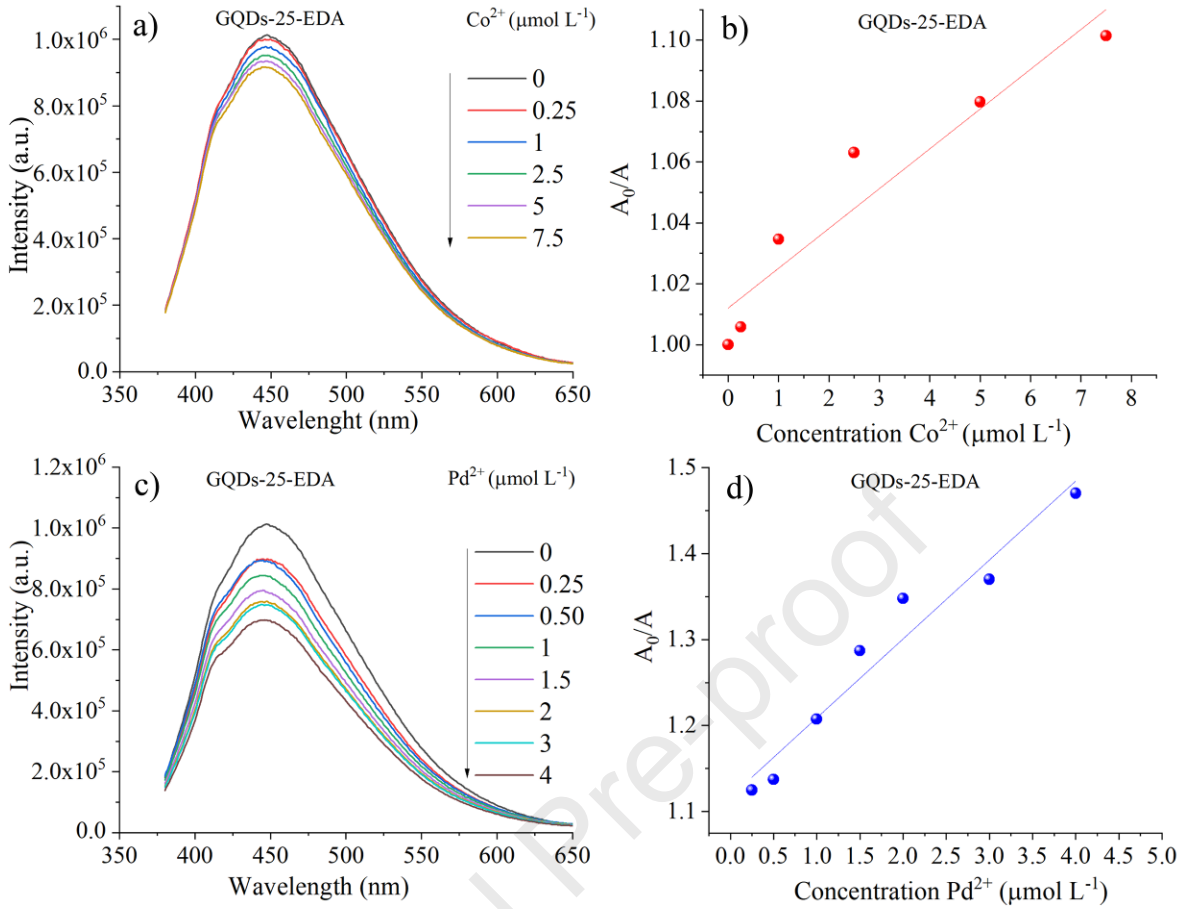

Figure 9. Emission spectra of the GQD-25-EDA (λ_{exc}=360 nm) with Pd^{2+} in the concentration range 0 – 4 µmol L^{-1} (c), and the Stern-Volmer plot (integrated area under emission peak versus concentration of Pd^{2+}) with the linear fitting curve (d).

Table 1. Results obtained using gamma-irradiated amino-functionalized GQDs compared to other optical probes for Pd^{2+} detection.

Types of probe	**Limit of detection (nmol L^{-1})**	**Linear range (µmol L^{-1})**	**Mechanism**
Conjugated polymer-based probe [52]	1000	/	turn-off probe for Pd^{2+} and Pt^{4+}
Metal-organic framework chemosensor (KFUPM-3) [51]	248	0-50	turn-off
Carbon nanoparticles (CNPs) [21]	58	35-100	turn-off dual probe for Pd^{2+} and Hg^{2+}

Red carbon dots (CDs) [53]	3290	20-160	turn-off probe for Pt^{2+}, Au^{2+} and Pd^{2+}
GQDs-25-EDA (presented work)	657	0.25-4	turn-off

Emission spectra of GQDs-25-EDA in the presence of Fe^{3+} ions at the concentration from 0 to 100 μmol L^{-1} showed a decrease in PL intensity with an increase in ion concentration (Figure 10a). Linear fitting of the Stern-Volmer plot (Figure 10b) it was found a linear response in the range 0-45 μmol L^{-1} (Figure 10c) and 0-100 μmol L^{-1} (Figure 10d). Linear relationship for both concentration ranges are described as $A_0/A = 0.97863 + 0.01129 [Fe^{3+}]$ and $A_0/A = 0.9825 + 0.0106 [Fe^{3+}]$, respectively. Values of R^2 were 0.991 and 0.987 for concentration ranges 0-45 μmol L^{-1} and 0-100 μmol L^{-1}, respectively. LODs were 2.55 μmol L^{-1} in the range of 0-45 μmol L^{-1} which is lower than the maximum level in drinking water (0.3 ppm or 5.37 μmol L^{-1}) permitted by the U.S. Environmental Protection Agency (EPA) [54] and 4.42 μmol L^{-1} for the range of 0-100 μmol L^{-1}. It can be observed that GQDs-25-EDA are more sensitive to the lower concentrations of Fe^{3+}. Table 2 summarizes the results obtained in this work compared with other recently published ones.

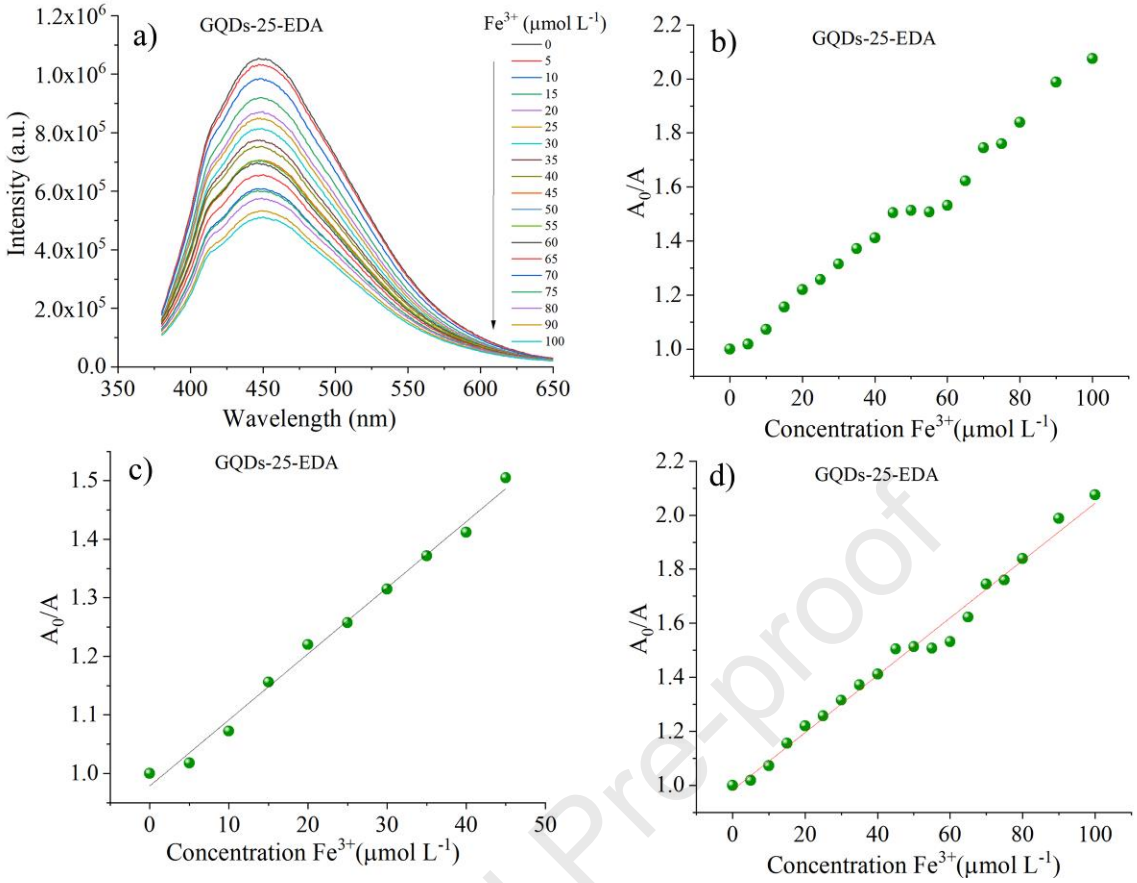

Figure 10. Emission spectra of the GQD-25-EDA recorded at λ_{exc}=360 nm in presence of Fe^{3+} ions in the concentration range 0-100 µmol L^{-1} (a), and the Stern-Volmer plot (integrated area under emission peak versus concentration of Fe^{3+}) (b) with the linear fitting curve for concentration ranges 0-50 µmol L^{-1} (c), and 0-100 µmol L^{-1} (d).

Table 2. Results obtained using different types of optical probes for Fe^{3+} based on fluorescence quenching.

Type of fluorescent Probe	**Limit of detection (µmolL^{-1})**	**Linear range (µmol L^{-1})**	**Mechanism**
CQDs [55]	3.70	0-20	turn-off
GQDs [56]	2.50	0-50	turn-off
N-GQDs [57]	2.37	1600-10000	turn-off
N-GQDs [54]	1.49	0-300	turn-off/turn-on probe for Fe^{3+} and ascorbic acid
GQDs-25-EDA (presented work)	2.55	0-45	turn-off

To observe the PL response of GQDs toward the presence of metal ions, we compared the relative fluorescent intensity (A/A_0) of GQDs-25-EDA without and in the presence of ions in concentrations of 5 μmol L^{-1} (Figure 11a), and 100 μmol L^{-1} (Figure 11b). At low ions concentration PL significantly decrease in the presence of Pd^{2+} while the other two ions did not lead to a considerable response. At the concentrations of 100 μmol L^{-1}, all three ions significantly quenched the PL of GQDs. These results are in the line with those previously presented and confirmed the highest sensitivity of GQDs-25-EDA toward Pd^{2+} at low concentrations.

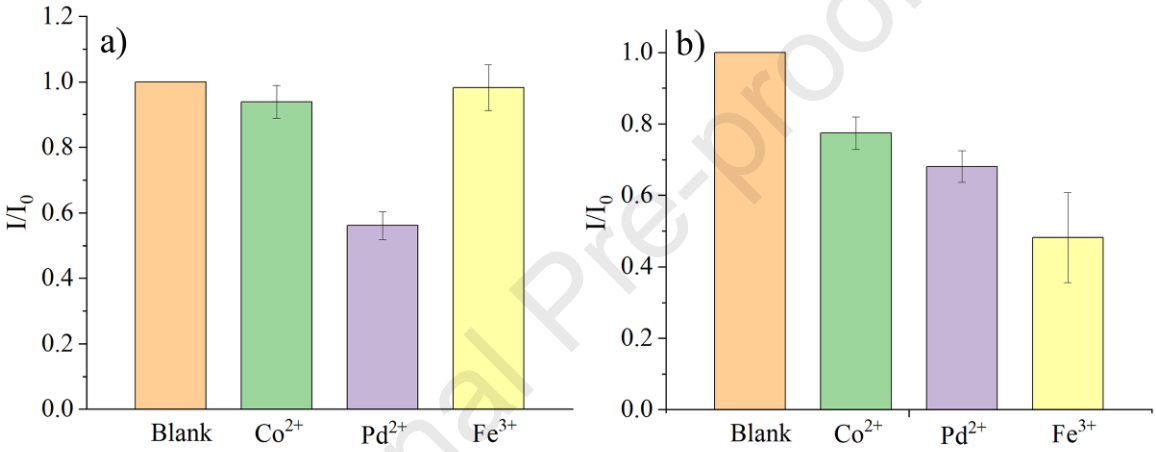

Figure 11. Relative fluorescence intensity of GQDs-25-EDA in the absence and the presence of Co^{2+}, Pd^{2+}, and Fe^{3+}, in the concentration of 5 μmol L^{-1} (a), and 100 μmol L^{-1} (b).

3.2.2. Investigation of morphological properties of irradiated GQDs in the presence of metal ions

To investigate changes in GQDs morphology in the presence of metal ions, AFM was used. In Figure 12, AFM images with height profiles of GQDs-50-EDA in the presence of Pd^{2+} (a) and Co^{2+} (b), and GQDs-25-EDA in presence of Fe^{3+} (c) were presented. According to several studies, metal ions induced the organization of GQDs into aggregates [58, 59]. Both Co^{2+} and Fe^{3+} led to the formation of uniformly dispersed GQD aggregates 50 or 30 nm high, respectively, while the Pd^{2+} caused the organization of GQDs in large aggregates higher than 100 nm. GQDs aggregate differently in the presence of metal ions with various molecular weights. Chen et al. investigated the hydrodynamic radius and aggregation rate of GQDs in presence of different cations (Na^+, K^+, Mg^{2+}, and Ca^{2+}) [59]. They found that heavier cations

lead to the faster formation of larger GQD aggregates compared to lighter-weight ions. Co^{2+} and Fe^{3+} (weights are 58.93 and 55.84 g mol^{-1}, respectively) are lighter than Pd^{2+} with a weight of 106.43 g mol^{-1}. Thus, this agrees with the previously reported trend. These results indicate a strong correlation between cation weight and the size of GQDs aggregates. A saturation of GQDs with Pd^{2+} at a concentration higher than 5 μmol L^{-1} also can be explained. This concentration of Pd^{2+} is efficient in inducing the organization of GQDs in large aggregates and consequently decreases the PL intensity.

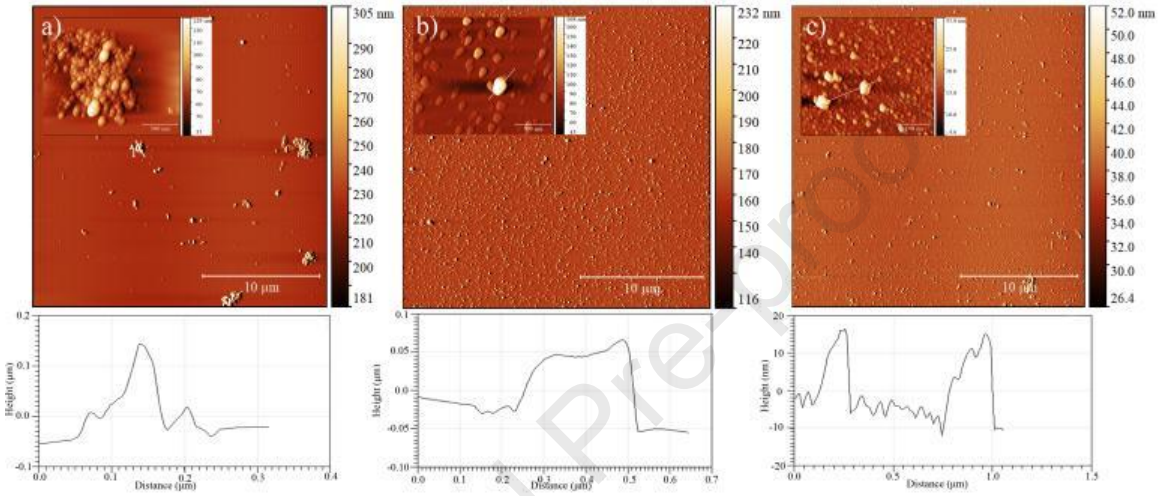

Figure 12. AFM images of GQDs-50-EDA in the presence of the Pd^{2+} and Co^{2+}, respectively (a, b) and GQDs-25-EDA in the presence of Fe^{3+} (c) with height profiles. The insets in the upper right corner of the images show aggregates of GQDs formed in the presence of metal ions.

3.2.3. Mechanism behind PL quenching GQDs with metal ions

Few studies proposed a mechanism of interaction between amino-functionalized GQDs and metal ions where metal ions show a tendency to form coordinative bonds with GQDs functional groups [5, 18, 60, 61]. Unfilled orbitals of metal ions were occupied by ligand electrons. Due to their surface functional groups, GQDs can create such bonds by donating electron pairs from functional groups or they are formed between metal ions and π-electrons. Another possibility is establishing the electrostatic interactions between metal ions and negatively charged functional groups, such as deprotonated carboxyl groups.

In the case of GQDs irradiated with EDA, zeta potentials at pH 7 for GQDs-25-EDA and GQDs-50-EDA were -18.8 and -15.1 mV, respectively, which indicated that dots are negatively charged due to the presence of deprotonated carboxylic groups at their surfaces. In

GQDs-200-EDA, protonated amino groups lead to the value of zeta potential +9.1 mV, but FTIR analysis was shown the presence of carboxyl groups in this sample [23]. PL measurements showed that the mixture of GQDs with metal ions reduced the PL intensity. To examine interactions between GQDs and ions in more detail, UV-Vis absorption spectra of GQDs-25-EDA in presence of Co^{2+}, Pd^{2+} and Fe^{3+} were recorded (Figures 13 a, b, and, c, respectively). In the case of the GQDs-25-EDA (Figure 13a), a band centered at 202 nm stems from the π-π* transition of aromatic C-C bonds. A shoulder band around 251 nm is attributed to the n-π* transition of C=O bonds in carbonyl functional groups. In the presence of the different concentrations of Co^{2+} ions, there is no obvious change in the spectra of GQDs-25-EDA (Figure 13a), although the AFM image (Figure 11b) confirmed GQDs aggregation. On the contrary, absorption spectra of GQDs-25-EDA recorded in the presence of Pd^{2+} and Fe^{3+} show significant changes. First, the intensity of absorbance increased in all cases. Enhance absorbance may be correlated with aggregation degree [62]. In the presence of Pd^{2+}, a band at 202 nm was shifted at 207, 213, 232, and 239 nm, at the 25, 50, 100, and 200 μmol L^{-1} of Pd^{2+}. Some researchers have reported the formation of π-complexes between Pd^{2+} and C=C sites of graphitized carbon materials [63], graphene [64], and activated carbon [65]. Therefore, these shifts can indicate complexation between π-sites on GQDs and Pd^{2+}. Also, the shoulder band around 251 nm has become more pronounced and also shifted at 235, 233, 275, and 278 nm, at the same concentrations of Pd^{2+}, due to changes in the chemical environment around C=O by complexation. A new broad absorption band located around 430 nm was also attributed to Pd (II) complex formation [66]. Similar spectra of the GQDs-25-EDA were obtained in the presence of Fe^{3+} ions. The broad absorption band around 251 nm was increased without significant shifting, but intensity enhancement may indicate the metal-ligand complex between Fe^{3+} and functional groups on the GQDs-25-EDA surface [67]. Additionally, the absorption band at 202 nm was increased and shifted at 207, 210, 214, and 219 nm in the presence of Fe^{3+} ions in concentrations of 25, 50, 100, and 200 μmol L^{-1}, respectively. Changes in this region may be attributed to cation-π interactions, due to the strong ability of metals to interact with the π electron cloud of graphene-based materials [68, 69]. According to these results and other reported studies, it can be assumed that GQDs aggregation in the presence of investigated ions occurs as a result of complexation with GQDs functional groups and cation-π interactions. Also, a linear increase of absorbance can be used for the colorimetric detection of cations [67]. PL of GQDs can be recovered by adding chelating agents such as ethylenediaminetetraacetate acid [70] or 3-amino-1,2,4-

triazole [71], which showed a higher affinity toward ions comper to GQD itself. This leads to the restoring of GQDs structure as well as their optical properties such as PL.

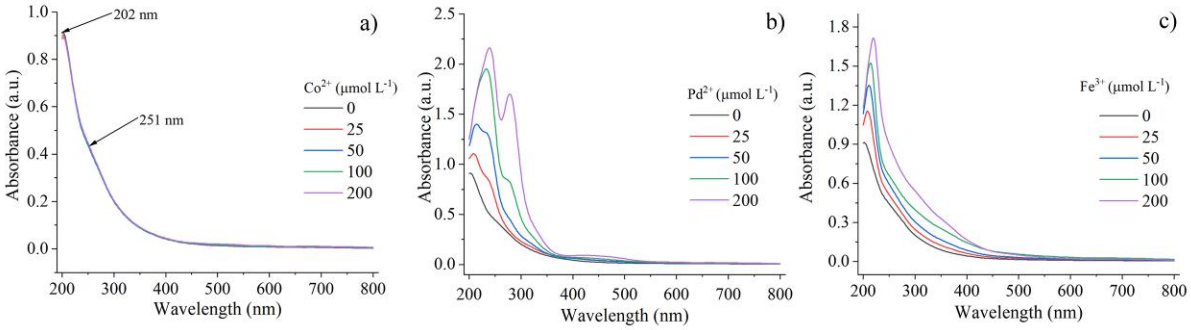

Figure 13. UV-Vis absorption spectra of GQDs-25-EDA in the presence of Co^{2+} (a), Pd^{2+} (b) and Fe^{3+} (c), in the concentration range 0-200 µmol L^{-1}.

3.2.4. Detection of Co^{2+}, Pd^{2+} and Fe^{3+} ions in real samples

To examine the applicability of GQDs-25-EDA as a PL probe for selected ions in real conditions, both tap and river water were used as real samples. Figure 14 shows the maximums of GQDs PL intensities measured in the tap water that contained Co^{2+} (a), Pd^{2+} (b), and Fe^{3+} ions (c) in the concentration range of 0-100 µmol L^{-1}. It can be seen that PL intensity decreased in the presence of these ions. Dependence curves of A_0/A from the concentration of Co^{2+}, Pd^{2+}, and Fe^{3+} ions were presented in Figures 14d, e, and f, respectively. A good linear correlation between A_0/A and ions concentrations was observed in the ranges of 25-100, and 10-100 µmol L^{-1}, for Co^{2+}, Pd^{2+}, and Fe^{3+}, respectively. R^2 values were 0.96, 0.97, and 0.93 for Co^{2+}, Pd^{2+}, and Fe^{3+} ions, respectively.

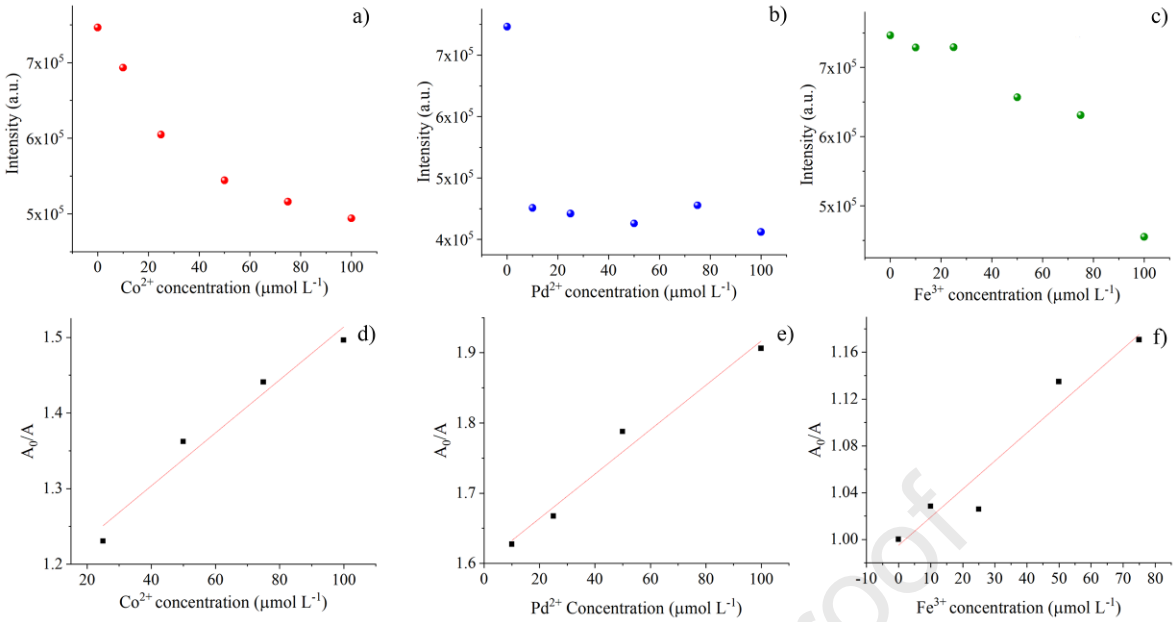

Figure 14. Maximums of GQDs PL intensities in tap water which contained different concentrations of Co^{2+} (a), Pd^{2+} (b), and Fe^{3+} ions (c). The A_0/A dependence of the concentration of Co^{2+} (d), Pd^{2+}(e), and Fe^{3+} (f).

Results obtained by recording a PL intensity of GQDs-25-EDA in the presence of the Co^{2+}, Pd^{2+}, and Fe^{3+} ions in river water are presented in Figures 15 a, b, and c, respectively. A decrease in PL intensities in the concentration range of 0-100 is observed in all spectra. Linearity between A_0/A and Co^{2+}, Pd^{2+}, and Fe^{3+} ions concentrations were detected in the ranges 10-100, 10-75, and 25-100 µmol L^{-1} (Figures 15d, e, and f), while R^2 values were 0.99, 0.92 and 0.97, respectively. Deviation from linearity of concentration 10 µmol L^{-1} can be attributed to experimental error.

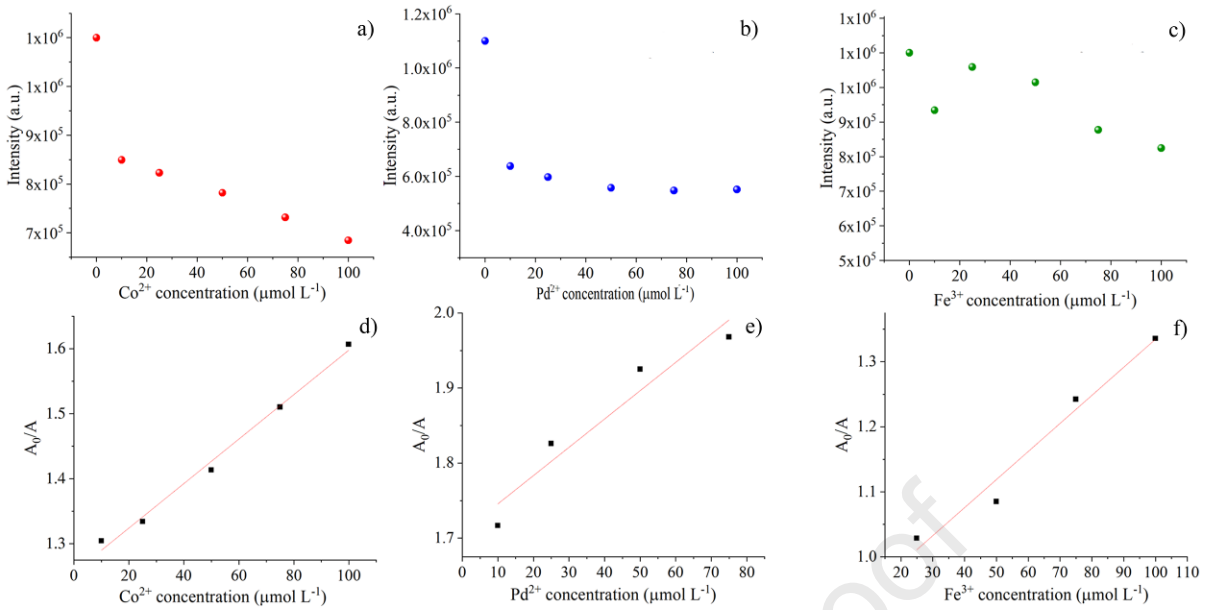

Figure 15. Maximums of GQDs PL intensities in river water which contained various concentrations of Co^{2+} (a), Pd^{2+} (b), and Fe^{3+} ions (c). The A_0/A dependence of the concentration of Co^{2+} (d), Pd^{2+}(e), and Fe^{3+} (f).

Results of the recovery test were presented in Table 3. Values obtained for R% determined by adding each ion in a concentration of 75 μmol L^{-1} in GQDs-25-EDA dispersion demonstrated the practical application of the tested PL probe.

Table 3. Results of recovery test obtained by determination of Co^{2+}, Pd^{2+}, and Fe^{3+} using GQDs-25-EDA as PL probe in real water samples.

Samples	Co^{2+} (μmol L^{-1})	Pd^{2+} (μmol L^{-1})	Fe^{3+} (μmol L^{-1})
Tap water	Added 75	Added 75	Added 75
	Found 79.2	/	Found 73.1
	R (%) 105.6		R (%) 97.5
River water	Added 75	Added 75	Added 75
	Found 74.3	Found 68.9	Found 78.6
	R (%) 99.1	R (%) 91.3	R (%) 104.8

The ability of GQDs-25-EDA to specifical interact with Co^{2+}, Pd^{2+} and Fe^{3+} ions was examined by measuring the emission peak intensity in the presence of these ions and compared with intensities in the presence of the Na^{+}, K^{+}, Ca^{2+}, Fe^{2+}, Cu^{2+}, Ni^{2+}, Zn^{2+}, and

Ag^{+}. Also, the mixture of all ions was studied. Results are presented in Figure 16 (a-c). These measurements indicate that there are no significant changes in GQDs PL intensity in the presence of the Na^{+}, K^{+}, Ca^{2+}, Fe^{2+}, Ni^{2+}, Zn^{2+}, and Ag^{+}. Only Cu^{2+} can affect Co^{2+} detection. PL intensities suggested that GQDs-25-EDA showed the highest selectivity toward Fe^{3+} ions.

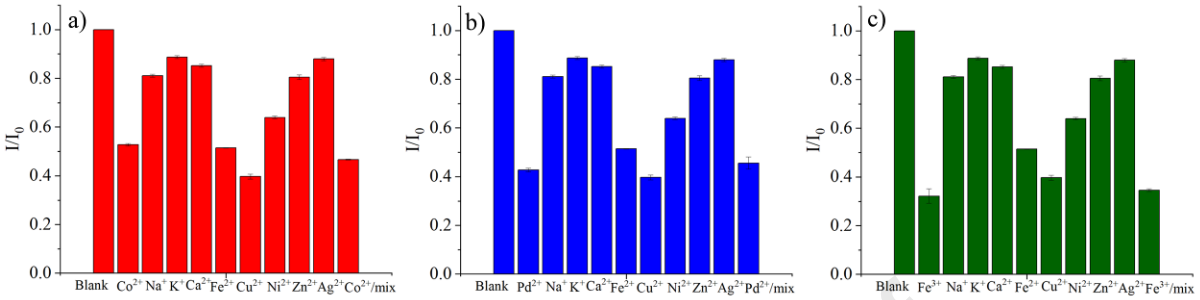

Figure 16. Selectivity of GQDs-25-EDA for detection of Co^{2+} (a), Pd^{2+} (b), and Fe^{3+} ions (c), in the presence of the Na^{+}, K^{+}, Ca^{2+}, Fe^{2+}, Cu^{2+}, Ni^{2+}, Zn^{2+}, and Ag^{+}.

In table 4, we listed results obtained for the detection of Co(II) ions using the same approach and we can see that our data are correlated with other studies.

Table 4. Comparison of results obtained using different types of PL probes for Co^{2+}.

Type of fluorescent Probe	Limit of detection ($\mu molL^{-1}$)	Linear range ($\mu mol\ L^{-1}$)	Mechanism
CDs [72]	0.39	1-200	turn-off
Au nanoclusters [73]	0.124	2-50	turn-off
N, S-GQDs [5]	1.25	0-40	turn-off
GQDs-25-EDA (presented work)	1.79	0-7.5	turn-off

3.3. Detection of malathion

In Figure 17a, PL spectra of GQDs-200-EDA in presence of the malathion in the concentration range of 0-140 ng mL^{-1} (0-0.4 $\mu mol\ L^{-1}$) are presented. Enhance of PL intensity is obvious, but in this range, linearity wasn't found.

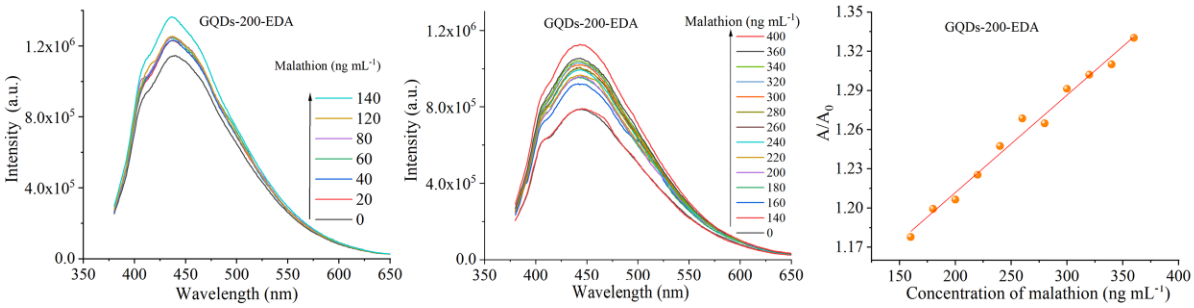

Figure 17. Emission spectra of the GQD-200-EDA in presence of malathion in the concentration range 0-140 ng mL^{-1} (a), and in the concentration range of 0-400 ng mL^{-1} (b), and Stern-Volmer plot (integrated area under emission peak versus concentration of malathion) with a linear fitting curve for concentration range 160-360 ng mL^{-1} (c).

Then, detection in the range of malathion concentration from 140 to 400 ng mL^{-1} (0.4-1.2 µmol L^{-1}) (Figure 17b) was tested. It can be seen that the PL intensity of GQDs-200-EDA increases linearly from 160-360 ng mL^{-1} (0.48 µmol L^{-1}-1 µmol L^{-1}) (Figure 17c) with R^2 = 0.986. The efficiency was calculated according to the Stern-Volmer equation. The calculated value for LOD was 31.41 ng mL^{-1} which corresponds to 0.094 µmol L^{-1}. LOD is much lower than the maximum acceptable concentration (MAC) for malathion in drinking water (100 µg L^{-1} (302.5 nmol L^{-1}) for children and 200 µg L^{-1} (605 nmol L^{-1}) for adults) according to EPA guidelines [74]. Thus, a highly sensitive platform for the detection of commercially available pesticides which shows poor solubility in water can be developed. In Table 5, this result with other results reported in the literature is compared.

Table 5. Comparison of results obtained using different types of PL probes for malathion.

Type of fluorescent probe	Limit of detection (nmol L^{-1})	Linear range (µmol L^{-1})	Mechanism
β-cyclodextrin@AgNPs + 2,3-Dihydro-5-oxo-5H-thiazolo[3,2-a]pyridine-7-carboxylic acid (D-TPCA) [75]	30	0.3-2.2	off-on
Upconversion fluorescent nanoparticles (UCNPs), gold nanoparticles (GNPs) and	1.42	0.01-0.1	turn-off

aptamer [76]			
GQDs [22]	500	80-120	turn-off/turn-on probe for Hg^{2+} and malathion
GQDs-200-EDA (presented work)	94	0.48-1	turn-on

In Table 6, the results collected by analyzing the PL intensity of GQDs in the presence of selected metal ions and malathion, the ranges of linear responses, coefficient of determination (R^2), and calculated values of LOD are listed.

Table 6. Parameters of linear fitting for GQDs PL probes.

Probe	Analyte	Linear range (μmol L^{-1})	R^2	LOD (μmol L^{-1})
GQDs-25-EDA	Co^{2+}	0-7.5	0.91	1.79
	Pd^{2+}	0-4	0.95	0.66
	Fe^{3+}	0-45	0.99	2.55
GQDs-50-EDA	Co^{2+}	0-15	0.98	2.79
GQDs-200-EDA	Co^{2+}	2.5-15	0.98	3.71
	malathion	0.48-1	0.98	0.094

3.4. Cytotoxicity investigation

Based on results obtained from the MTT assay and LIVE/DEAD cytotoxicity test, the effects of investigated GQDs on the viability of MRC-cells were evaluated. As shown in Figure 18 which are presents results from the MTT assay, all tested samples present similar effects on the MRC-5 cells with viability higher than 71 %. Treatments with all analyzed concentrations of p-GQDs (a), GQD-25-EDA (b), GQD-50-EDA (c), and GQD-200-EDA (d) at all three timepoints showed MRC-5 cell viability above 80 % which is considered as non-cytotoxicity [49]. In the treatments with GQD-25-EDA only a sample of 25 μg mL^{-1} presented weak cytotoxicity (71 %) after 24h of treatment. Every other concentration of GQD-25-EDA in all analyzed time points showed non-cytotoxicity against MRC-5 cells.

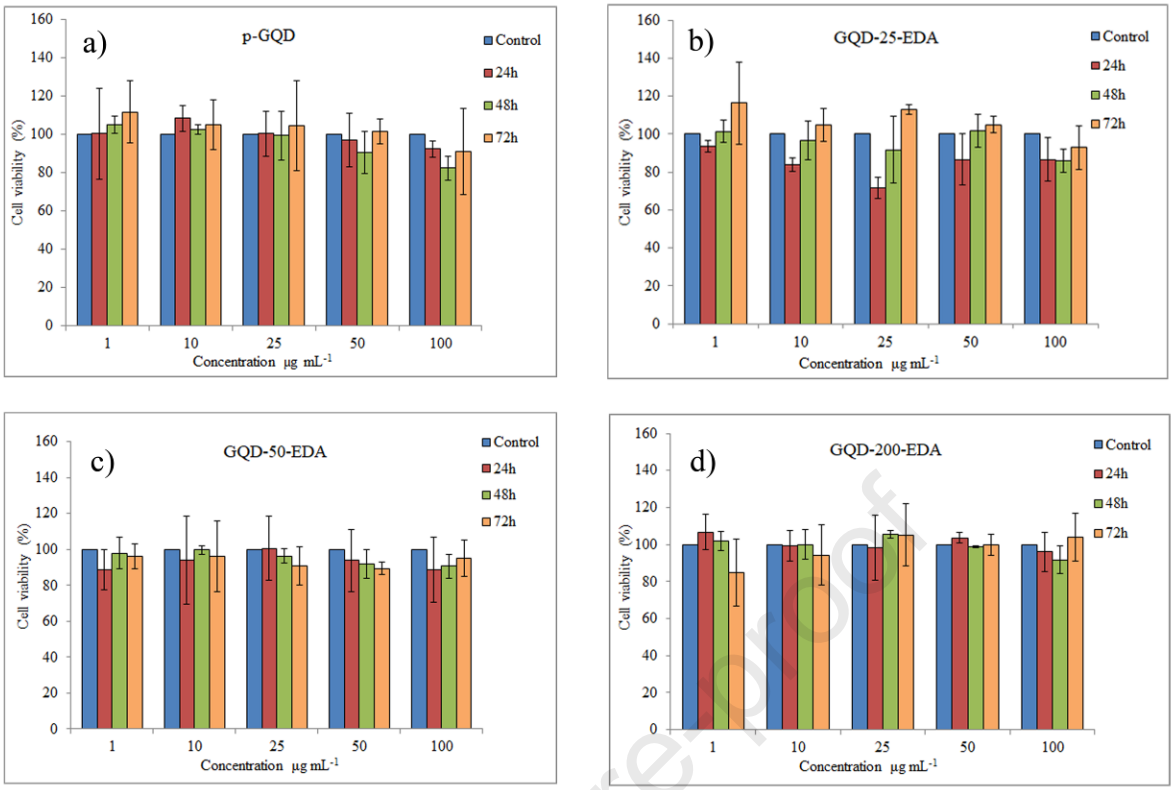

Figure 18. Effects of p-GQD, GQD-25-EDA, GQD-50-EDA, and GQD-200-EDA on the viability of MRC-5 cells assessed by MTT test. MRC-5 cells were treated with increasing concentrations (1, 10, 25, 50, and 100 µg mL^{-1}) of p-GQDs (a), GQD-25-EDA (b), GQD-50-EDA (c), and GQD-200-EDA (d) for the indicated periods of time (24, 48, and 72h). Obtained results were presented as percent relative to the value obtained for MRC-5 cells treated with vehicle control (methanol) and set at 100 %. Mean values of relative viability rates were compared using Student's test. Values are shown as means ± SD from three independent experiments (n = 3); $p < 0.05$ versus respective control.

In the line with the results obtained in the MTT assay, the LIVE/DEAD cell test showed that none of the tested samples of GQDs at concentrations of 100 µg mL^{-1} have a cytotoxic effect on MRC-5 cells (Figure 19, panels a, b, c, d, and e).

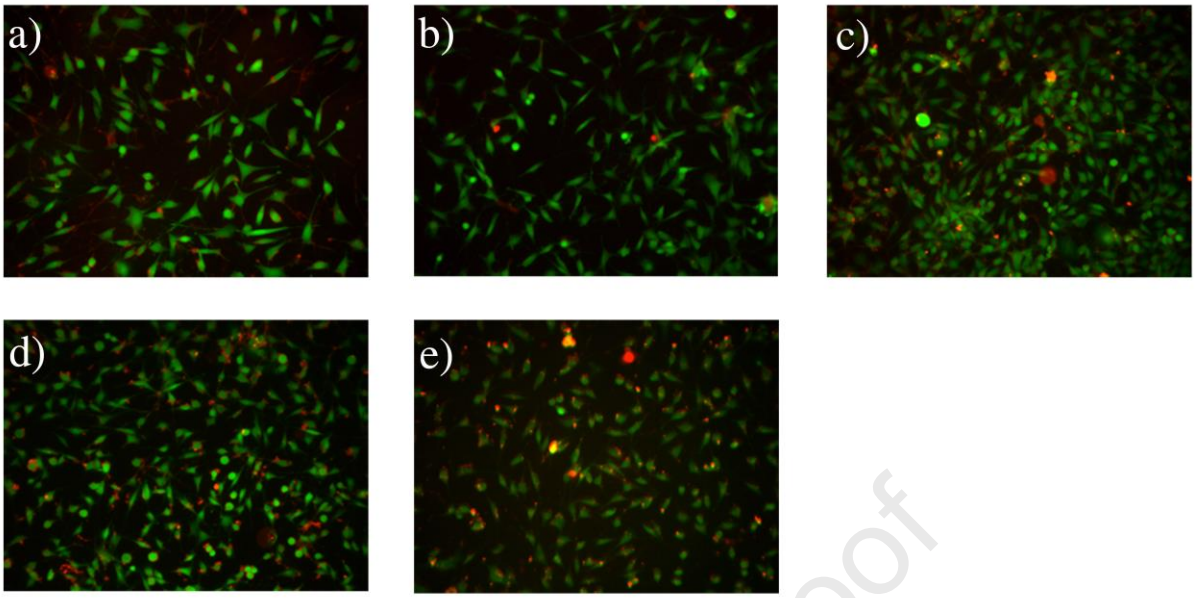

Figure 19. Fluorescence microscopy of control MRC-5 cells a) and cells incubated 48h with 100 μg mL^{-1} of b) p-GQD, c) GQD-25-EDA, d) GQD-50-EDA and e) GQD-200-EDA. Simultaneous staining with green-fluorescent and red-fluorescent dye discriminates live (green) from dead (red) cells. All panels share the scale bar reported in panel a), which stands for 100 μm.

4. Conclusion

In this work, GQDs modified by gamma irradiation are studied as potential probes for Co^{2+}, Pd^{2+}, Fe^{3+}, and malathion detection. LODs values were evaluated as 1.79, 2.79, and 3.71 μmol L^{-1} in the case of Co^{2+} for GQDs-25-EDA, GQDs-50-EDA, and GQDs-200-EDA, respectively. For the first time, GQDs were successfully employed in Pd^{2+} detection in water with very low LOD (0.657 μmol L^{-1}). Furthermore, GQDs-25-EDA expressed a great potential as a turn-off probe for Fe^{3+} in water with LODs of 2.55 μmol L^{-1}. Excellent results were observed when dots were mixed with malathion in ethanol: for the first time, the linear relation between insecticide concentration and PL intensity of solely GQDs was established. GQDs-200-EDA turned out to be an outstanding PL turn-on probe for malathion with a LOD value of 94 nmol L^{-1}. Currently, this is the most simple and the only direct probe for PL detection of malathion with GQDs. Cytotoxicity assays showed that GQDs-EDA are non-toxic and safe materials. Thus, gamma-irradiated amino-functionalized GQDs are sensitive, non-toxic, eco-friendly, and low-cost material for rapid PL sensing of selected metal ions in water and insecticide malathion in ethanol.

5. Acknowledgements

The research was supported by the Science Fund of the Republic of Serbia, #7741955, *Are photoactive nanoparticles salvation for global infectional treath?* - PHOTOGUN4MICROBES and by the Ministry of Education, Science and Technological Development of the Republic of Serbia [grant number 451-03-68/2022-14/200017, 451-03-68/2022-14/200026, and 451-03-68/2022-14/200042]. The Italian Ministry of University and Research (MURST, ex-MIUR) is acknowledged by A.B. for funding his research activities (PON "AIM: Attrazione e Mobilità Internazionale", call AIM1809078-2, CUP B78D19000280001). The Advanced Technologies Network (ATeN) Center (University of Palermo; project "Mediterranean Center for Human Health Advanced Biotechnologies (CHAB)", PON R&C 2007-2013) is also acknowledged for hospitality and service.

6. References

[1] M. Jaishankar, T. Tseten, N. Anbalagan, B.B. Mathew, K.N. Beeregowda, Toxicity, mechanism and health effects of some heavy metals, Interdiscip Toxicol, 7 (2014) 60-72. https://doi.org/10.2478/intox-2014-0009.

[2] A. Sharma, A. Shukla, K. Attri, M. Kumar, P. Kumar, A. Suttee, G. Singh, R.P. Barnwal, N. Singla, Global trends in pesticides: A looming threat and viable alternatives, Ecotoxicology and Environmental Safety, 201 (2020) 110812. https://doi.org/10.1016/j.ecoenv.2020.110812.

[3] Q. Ma, J. Song, S. Wang, J. Yang, Y. Guo, C. Dong, A general sensing strategy for detection of Fe3+ by using amino acid-modified graphene quantum dots as fluorescent probe, Applied Surface Science, 389 (2016) 995-1002. https://doi.org/10.1016/j.apsusc.2016.08.039.

[4] W. Xuan, L. Ruiyi, F. Saiying, L. Zaijun, W. Guangli, G. Zhiguo, L. Junkang, D-penicillamine-functionalized graphene quantum dots for fluorescent detection of Fe3+ in iron supplement oral liquids, Sensors and Actuators B: Chemical, 243 (2017) 211-220. https://doi.org/10.1016/j.snb.2016.11.150.

[5] W. Boonta, C. Talodthaisong, S. Sattayaporn, C. Chaicham, A. Chaicham, S. Sahasithiwat, L. Kangkaew, S. Kulchat, The synthesis of nitrogen and sulfur co-doped graphene quantum dots for fluorescence detection of cobalt(ii) ions in water, Materials Chemistry Frontiers, 4 (2020) 507-516. https://doi.org/10.1039/C9QM00587K.

[6] Q. Sun, Y. Qiu, J. Chen, F.-S. Wu, X.-G. Luo, Y.-R. Guo, X.-Y. Han, D.-W. Wang, A colorimetric and fluorescence turn-on probe for the detection of palladium in aqueous solution and its application in vitro and in vivo, Spectrochimica Acta Part A: Molecular and Biomolecular Spectroscopy, 239 (2020) 118547. https://doi.org/10.1016/j.saa.2020.118547.
[7] J. Kaushal, M. Khatri, S.K. Arya, A treatise on Organophosphate pesticide pollution: Current strategies and advancements in their environmental degradation and elimination, Ecotoxicology and Environmental Safety, 207 (2021) 111483. https://doi.org/10.1016/j.ecoenv.2020.111483.
[8] A.M. Badr, Organophosphate toxicity: updates of malathion potential toxic effects in mammals and potential treatments, Environmental science and pollution research international, 27 (2020) 26036-26057. 10.1007/s11356-020-08937-4.
[9] N. Sohal, B. Maity, S. Basu, Recent advances in heteroatom-doped graphene quantum dots for sensing applications, RSC Advances, 11 (2021) 25586-25615. https://doi.org/10.1039/D1RA04248C.
[10] M. Milenković, A. Mišović, D. Jovanović, A. Popović Bijelić, G. Ciasca, S. Romanò, A. Bonasera, M. Mojsin, J. Pejić, M. Stevanović, S. Jovanović, Facile Synthesis of L-Cysteine Functionalized Graphene Quantum Dots as a Bioimaging and Photosensitive Agent, Nanomaterials, 11 (2021) 1879. https://doi.org/10.3390/nano11081879.
[11] S. Dorontić, S. Jovanović, A. Bonasera, Shedding Light on Graphene Quantum Dots: Key Synthetic Strategies, Characterization Tools, and Cutting-Edge Applications, Materials, 14 (2021) 6153. https://doi.org/10.3390/ma14206153.
[12] B. Lyu, H.-J. Li, F. Xue, L. Sai, B. Gui, D. Qian, X. Wang, J. Yang, Facile, gram-scale and eco-friendly synthesis of multi-color graphene quantum dots by thermal-driven advanced oxidation process, Chemical Engineering Journal, 388 (2020) 124285. https://doi.org/10.1016/j.cej.2020.124285.
[13] A. Xu, G. Wang, Y. Li, H. Dong, S. Yang, P. He, G. Ding, Carbon-Based Quantum Dots with Solid-State Photoluminescent: Mechanism, Implementation, and Application, 16 (2020) 2004621. https://doi.org/10.1002/smll.202004621.
[14] S. Yang, J. Sun, X. Li, W. Zhou, Z. Wang, P. He, G. Ding, X. Xie, Z. Kang, M. Jiang, Large-scale fabrication of heavy doped carbon quantum dots with tunable-photoluminescence and sensitive fluorescence detection, J Mater Chem A, 2 (2014) 8660-8667. https://doi.org/10.1039/C4TA00860J.
[15] S. Yang, W. Li, C. Ye, G. Wang, H. Tian, C. Zhu, P. He, G. Ding, X. Xie, Y. Liu, Y. Lifshitz, S.-T. Lee, Z. Kang, M. Jiang, C3N—A 2D Crystalline, Hole-Free, Tunable-Narrow-

Bandgap Semiconductor with Ferromagnetic Properties, 29 (2017) 1605625. https://doi.org/10.1002/adma.201605625.

[16] J. Sun, S. Yang, Z. Wang, H. Shen, T. Xu, L. Sun, H. Li, W. Chen, X. Jiang, G. Ding, Z. Kang, X. Xie, M. Jiang, Ultra-High Quantum Yield of Graphene Quantum Dots: Aromatic-Nitrogen Doping and Photoluminescence Mechanism, 32 (2015) 434-440. https://doi.org/10.1002/ppsc.201400189.

[17] J. Li, S. Yang, Z. Liu, G. Wang, P. He, W. Wei, M. Yang, Y. Deng, P. Gu, X. Xie, Z. Kang, G. Ding, H. Zhou, X. Fan, Imaging Cellular Aerobic Glycolysis using Carbon Dots for Early Warning of Tumorigenesis, Adv Mater, 33 (2021) e2005096. https://doi.org/10.1002/adma.202005096.

[18] N. Wang, Z.X. Liu, R.S. Li, H.Z. Zhang, C.Z. Huang, J. Wang, The aggregation induced emission quenching of graphene quantum dots for visualizing the dynamic invasions of cobalt(ii) into living cells, Journal of Materials Chemistry B, 5 (2017) 6394-6399. https://doi.org/10.1039/C7TB01316G.

[19] Z. Wang, D. Chen, B. Gu, B. Gao, Z. Liu, Y. Yang, Q. Guo, X. Zheng, G. Wang, Yellow emissive nitrogen-doped graphene quantum dots as a label-free fluorescent probe for Fe3+ sensing and bioimaging, Diamond and Related Materials, 104 (2020) 107749. https://doi.org/10.1016/j.diamond.2020.107749.

[20] S. Mohapatra, M.K. Bera, R.K. Das, Rapid “turn-on” detection of atrazine using highly luminescent N-doped carbon quantum dot, Sensors and Actuators B: Chemical, 263 (2018) 459-468. https://doi.org/10.1016/j.snb.2018.02.155.

[21] V. Sharma, A. Saini, M. Shaikh, Multicolour fluorescent carbon nanoparticle probes for live cell imaging cum dual palladium and mercury sensor, J. Mater. Chem. B, 4 (2016). https://doi.org/10.1039/C6TB00238B.

[22] M. Roushani, S. Kohzadi, S. Haghjoo, A. Azadbakht, Dual detection of Malation and Hg (II) by Fluorescence switching of Graphene Quantum Dots, Environmental Nanotechnology, Monitoring & Management, 10 (2018). https://doi.org/10.1016/j.enmm.2018.08.002.

[23] S. Jovanović, S. Dorontić, D. Jovanović, G. Ciasca, M. Budimir, A. Bonasera, M. Scopelliti, O. Marković, B. Todorović Marković, Gamma irradiation of graphene quantum dots with ethylenediamine: Antioxidant for ion sensing, Ceramics International, 46 (2020) 23611-23622. https://doi.org/10.1016/j.ceramint.2020.06.133.

[24] Q.L. Zhao, Z.L. Zhang, B.H. Huang, J. Peng, M. Zhang, D.W. Pang, Facile preparation of low cytotoxicity fluorescent carbon nanocrystals by electrooxidation of graphite, Chem Commun (Camb), (2008) 5116-5118. https://doi.org/10.1039/b812420e.

[25] A.T.R. Williams, S.A. Winfield, J.N. Miller, Relative fluorescence quantum yields using a computer-controlled luminescence spectrometer, Analyst, 108 (1983) 1067-1071. https://doi.org/10.1039/AN9830801067.

[26] D. Magde, G.E. Rojas, P.G. Seybold, Solvent Dependence of the Fluorescence Lifetimes of Xanthene Dyes, Photochem. Photobiol., 70 (1999) 737-744. https://doi.org/10.1111/j.1751-1097.1999.tb08277.x.

[27] Z. Liu, Z. Mo, X. Niu, X. Yang, Y. Jiang, P. Zhao, N. Liu, R. Guo, Highly sensitive fluorescence sensor for mercury(II) based on boron- and nitrogen-co-doped graphene quantum dots, Journal of Colloid and Interface Science, 566 (2020) 357-368. https://doi.org/10.1016/j.jcis.2020.01.092.

[28] M. Vedamalai, P. Prakash, C.-W. Wang, Y.-t. Tseng, L.-C. Ho, C.-C. Shih, H.-T. Chang, Carbon nanodots prepared from o-phenylenediamine for sensing of Cu2+ ions in cells, Nanoscale, 6 (2014). https://doi.org/10.1039/C4NR03213F.

[29] Z.M. Marković, S.P. Jovanović, P.Z. Mašković, M. Danko, M. Mičušík, V.B. Pavlović, D.D. Milivojević, A. Kleinová, Z. Špitalský, B.M. Todorović Marković, Photo-induced antibacterial activity of four graphene based nanomaterials on a wide range of bacteria, RSC Advances, 8 (2018) 31337-31347. https://doi.org/10.1039/C8RA04664F.

[30] P.-C. Yang, Y.-X. Ting, S. Gu, Y. Ashraf Gandomi, J. Li, C.-T. Hsieh, Effect of Solvent on Fluorescence Emission from Polyethylene Glycol-Coated Graphene Quantum Dots under Blue Light Illumination, Nanomaterials, 11 (2021) 1383. https://doi.org/10.3390/nano11061383.

[31] T. Pillar-Little, D.Y. Kim, Differentiating the impact of nitrogen chemical states on optical properties of nitrogen-doped graphene quantum dots, RSC Advances, 7 (2017) 48263-48267. https://doi.org/10.1039/C7RA09252K.

[32] J. Zhu, Y. Tang, G. Wang, J. Mao, Z. Liu, T. Sun, M. Wang, D. Chen, Y. Yang, J. Li, Y. Deng, S. Yang, Green, Rapid, and Universal Preparation Approach of Graphene Quantum Dots under Ultraviolet Irradiation, ACS Applied Materials & Interfaces, 9 (2017) 14470-14477. https://doi.org/10.1021/acsami.6b11525.

[33] Z. Zhong, S. Long, Y. Fu, Y. Xu, γ-irradiation stability of anhydrous ethylenediamine, Journal of Radiation Research and Radiation Processing, 23 (2005) 287-291.

[34] P. Rona, M. Anbar, THE RADIOLYSIS OF ALKYL DIAMINES IN OXYGEN SATURATED DILUTE AQUEOUS SOLUTIONS. Progress Report, Israel. Atomic Energy Commission. Soreq Research Establishment, Rehovoth, 1963.

[35] B. Zhang, L. Li, Z. Wang, S. Xie, Y. Zhang, Y. Shen, M. Yu, B. Deng, Q. Huang, C. Fan, J. Li, Radiation induced reduction: An effective and clean route to synthesize functionalized graphene, Journal of Materials Chemistry, 22 (2012) 7775-7781. https://doi.org/10.1039/c2jm16722k.

[36] S.P. Jovanović, Z. Syrgiannis, Z.M. Marković, A. Bonasera, D.P. Kepić, M.D. Budimir, D.D. Milivojević, V.D. Spasojević, M.D. Dramićanin, V.B. Pavlović, B.M. Todorović Marković, Modification of Structural and Luminescence Properties of Graphene Quantum Dots by Gamma Irradiation and Their Application in a Photodynamic Therapy, ACS Applied Materials and Interfaces, 7 (2015) 25865-25874. https://doi.org/10.1021/acsami.5b08226.

[37] S. Jovanović, Gamma rays in carbon-based nanomaterials modification, in: J. Brock (Ed.) Gamma Irradiation: Properties, Effects and Development of New Materials, Nova Science Publishers, Inc., Hauppauge, NY 11788 USA, 2021, pp. 65-121.

[38] M. Chen, Y. Xie, H. Chen, Z. Qiao, Y. Qian, Preparation and Characterization of Metal Sulfides in Ethylenediamine under Ambient Conditions through a γ-Irradiation Route, Journal of Colloid and Interface Science, 237 (2001) 47-53. https://doi.org/10.1006/jcis.2001.7436.

[39] Y.L. He, J.H. Li, L.F. Li, J.B. Chen, J.Y. Li, The synergy reduction and self-assembly of graphene oxide via gamma-ray irradiation in an ethanediamine aqueous solution, Nuclear Science and Techniques, 27 (2016). https://doi.org/10.1007/s41365-016-0068-8.

[40] S. Le Caër, Water Radiolysis: Influence of Oxide Surfaces on H2 Production under Ionizing Radiation, 3 (2011) 235-253. https://doi.org/10.3390/w3010235.

[41] J. Belloni, Nucleation, growth and properties of nanoclusters studied by radiation chemistry: Application to catalysis, Catalysis Today, 113 (2006) 141-156. https://doi.org/10.1016/j.cattod.2005.11.082.

[42] J. Li, B. Zhang, L. Li, H. Ma, M. Yu, J. Li, γ-ray irradiation effects on graphene oxide in an ethylenediamine aqueous solution, Radiation Physics and Chemistry, 94 (2014) 80-83. https://doi.org/10.1016/j.radphyschem.2013.06.029.

[43] Y.-L. He, J.-H. Li, L.-F. Li, J.-B. Chen, J.-Y. Li, The synergy reduction and self-assembly of graphene oxide via gamma-ray irradiation in an ethanediamine aqueous solution, Nuclear Science and Techniques, 27 (2016) 61. https://doi.org/10.1007/s41365-016-0068-8.

[44] H. Huang, X. Tang, F. Chen, J. Liu, H. Li, D. Chen, Graphene damage effects on radiation-resistance and configuration of copper–graphene nanocomposite under irradiation: A molecular dynamics study, Scientific Reports, 6 (2016) 39391. https://doi.org/10.1038/srep39391.

[45] D. Kleut, S. Jovanović, Z. Marković, D. Kepić, D. Tošić, N. Romčević, M. Marinović-Cincović, M. Dramićanin, I. Holclajtner-Antunović, V. Pavlović, G. Dražić, M. Milosavljević, B. Todorović Marković, Comparison of structural properties of pristine and gamma irradiated single-wall carbon nanotubes: Effects of medium and irradiation dose, Materials Characterization, 72 (2012) 37-45. http://dx.doi.org/10.1016/j.matchar.2012.07.002.

[46] B. Li, Y. Feng, K. Ding, G. Qian, X. Zhang, J. Zhang, The effect of gamma ray irradiation on the structure of graphite and multi-walled carbon nanotubes, Carbon, 60 (2013) 186-192. https://doi.org/10.1016/j.carbon.2013.04.012.

[47] M. Algarra, V. Moreno, J.M. Lázaro-Martínez, E. Rodríguez-Castellón, J. Soto, J. Morales, A. Benítez, Insights into the formation of N doped 3D-graphene quantum dots. Spectroscopic and computational approach, Journal of Colloid and Interface Science, 561 (2020) 678-686. https://doi.org/10.1016/j.jcis.2019.11.044.

[48] F. Temerov, A. Belyaev, B. Ankudze, T. Pakkanen, Preparation and Photoluminescence Properties of Graphene Quantum Dots by Decomposition of Graphene-encapsulated Metal Nanoparticles Derived from Kraft Lignin and Transition Metal Salts, Journal of Luminescence, 206 (2018). https://doi.org/10.1016/j.jlumin.2018.10.093.

[49] C. Zhu, S. Yang, G. Wang, R. Mo, P. He, J. Sun, Z. Di, N. Yuan, J. Ding, G. Ding, X. Xie, Negative induction effect of graphite N on graphene quantum dots: tunable band gap photoluminescence, J Mater Chem C, 3 (2015) 8810-8816. https://doi.org/10.1039/C5TC01933H.

[50] T. Anusuya, V. Kumar, V. Kumar, Hydrophilic graphene quantum dots as turn-off fluorescent nanoprobes for toxic heavy metal ions detection in aqueous media, Chemosphere, 282 (2021) 131019. https://doi.org/10.1016/j.chemosphere.2021.131019.

[51] A. Helal, H.L. Nguyen, A. Al-Ahmed, K.E. Cordova, Z.H. Yamani, An Ultrasensitive and Selective Metal–Organic Framework Chemosensor for Palladium Detection in Water, Inorganic Chemistry, 58 (2019) 1738-1741. https://doi.org/10.1021/acs.inorgchem.8b02871.

[52] M.P. Tracey, D. Pham, K. Koide, Fluorometric imaging methods for palladium and platinum and the use of palladium for imaging biomolecules, Chemical Society Reviews, 44 (2015) 4769-4791. https://doi.org/10.1039/C4CS00323C.

[53] W. Gao, H. Song, X. Wang, X. Liu, X. Pang, Y. Zhou, B. Gao, X. Peng, Carbon Dots with Red Emission for Sensing of Pt2+, Au3+, and Pd2+ and Their Bioapplications in Vitro and in Vivo, ACS Applied Materials & Interfaces, 10 (2018) 1147-1154. https://doi.org/10.1021/acsami.7b16991.

[54] L. Zhu, D. Li, H. Lu, S. Zhang, H. Gao, Lignin-based fluorescence-switchable graphene quantum dots for Fe3+ and ascorbic acid detection, International Journal of Biological Macromolecules, 194 (2022) 254-263. https://doi.org/10.1016/j.ijbiomac.2021.11.199.
[55] F. Wu, H. Su, K. Wang, W.K. Wong, X. Zhu, Facile synthesis of N-rich carbon quantum dots from porphyrins as efficient probes for bioimaging and biosensing in living cells, International journal of nanomedicine, 12 (2017) 7375-7391. https://doi.org/10.2147/ijn.s147165.
[56] A. Abbas, T.A. Tabish, S.J. Bull, T.M. Lim, A.N. Phan, High yield synthesis of graphene quantum dots from biomass waste as a highly selective probe for Fe(3+) sensing, Sci Rep, 10 (2020) 21262-21262. https://doi.org/10.1038/s41598-020-78070-2.
[57] F. Lu, Y.-h. Zhou, L.-h. Wu, J. Qian, S. Cao, Y.-f. Deng, Y. Chen, Highly Fluorescent Nitrogen-Doped Graphene Quantum Dots' Synthesis and Their Applications as Fe(III) Ions Sensor, International Journal of Optics, 2019 (2019) 8724320. https://doi.org/10.1155/2019/8724320.
[58] J.M. Bai, L. Zhang, R.P. Liang, J.D. Qiu, Graphene quantum dots combined with europium ions as photoluminescent probes for phosphate sensing, Chemistry, 19 (2013) 3822-3826. https://doi.org/10.1002/chem.201204295.
[59] Q. Li, B. Chen, B. Xing, Aggregation Kinetics and Self-Assembly Mechanisms of Graphene Quantum Dots in Aqueous Solutions: Cooperative Effects of pH and Electrolytes, Environmental Science & Technology, 51 (2017) 1364-1376. https://doi.org/10.1021/acs.est.6b04178.
[60] Y. Fu, G. Gao, J. Zhi, Electrochemical synthesis of multicolor fluorescent N-doped graphene quantum dots as a ferric ion sensor and their application in bioimaging, Journal of Materials Chemistry B, 7 (2019) 1494-1502. https://doi.org/10.1039/C8TB03103G.
[61] L. Li, L. Li, C. Wang, K. Liu, R. Zhu, H. Qiang, Y. Lin, Synthesis of nitrogen-doped and amino acid-functionalized graphene quantum dots from glycine, and their application to the fluorometric determination of ferric ion, Microchimica Acta, 182 (2015) 763-770. https://doi.org/10.1007/s00604-014-1383-6.
[62] X.D. Zhang, J. Chen, Y. Min, G.B. Park, X. Shen, S.S. Song, Y.M. Sun, H. Wang, W. Long, J. Xie, K. Gao, L. Zhang, S. Fan, F. Fan, U. Jeong, Metabolizable Bi<inf>2</inf>Se<inf>3</inf> nanoplates: Biodistribution, toxicity, and uses for cancer radiation therapy and imaging, Advanced Functional Materials, 24 (2014) 1718-1729. https://doi.org/10.1002/adfm.201302312.

[63] A. Wieckowski, E. Savinova, Catalysis and electrocatalysis at nanoparticle surfaces / edited by Andrzej Wieckowski, Elena R. Savinova, Constantinos G. Vayenas, SERBIULA (sistema Librum 2.0), (2005).
[64] J. Yang, C. Tian, L. Wang, T. Tan, J. Yin, B. Wang, H. Fu, In Situ Reduction, Oxygen Etching, and Reduction Using Formic Acid: An Effective Strategy for Controllable Growth of Monodisperse Palladium Nanoparticles on Graphene, ChemPlusChem, 77 (2012) 301-307. https://doi.org/10.1002/cplu.201100058.
[65] M. Wojnicki, R.P. Socha, Z. Pędzich, K. Mech, T. Tokarski, K. Fitzner, Palladium(II) Chloride Complex Ion Recovery from Aqueous Solutions Using Adsorption on Activated Carbon, Journal of Chemical & Engineering Data, 63 (2018) 702-711. https://doi.org/10.1021/acs.jced.7b00885.
[66] N. Iranpoor, S. Rahimi, F. Panahi, In situ generated and stabilized Pd nanoparticles by N2,N4,N6-tridodecyl-1,3,5-triazine-2,4,6-triamine (TDTAT) as reactive and efficient catalyst for Suzuki-Miyaura reaction in water, RSC Advances, 6 (2015). https://doi.org/10.1039/C5RA24120K.
[67] X. Zhou, G. Zhao, X. Tan, X. Qian, T. Zhang, J. Gui, L. Yang, X. Xie, Nitrogen-doped carbon dots with high quantum yield for colorimetric and fluorometric detection of ferric ions and in a fluorescent ink, Microchimica Acta, 186 (2019) 67. https://doi.org/10.1007/s00604-018-3176-9.
[68] G. Zhao, H. Zhu, Cation–π Interactions in Graphene-Containing Systems for Water Treatment and Beyond, Advanced Materials, 32 (2020) 1905756. https://doi.org/10.1002/adma.201905756.
[69] R. Liu, X. Zhu, B. Chen, A New Insight of Graphene oxide-Fe(III) Complex Photochemical Behaviors under Visible Light Irradiation, Scientific Reports, 7 (2017) 40711. https://doi.org/10.1038/srep40711.
[70] W. Zhang, J. Gan, Synthesis of blue-photoluminescent graphene quantum dots/polystyrenic anion-exchange resin for Fe(III) detection, Applied Surface Science, 372 (2016) 145-151. https://doi.org/10.1016/j.apsusc.2016.02.248.
[71] S. Dorontic, A. Bonasera, M. Scopelliti, O. Markovic, D. Bajuk Bogdanović, G. Ciasca, S. Romanò, I. Dimkić, M. Budimir, D. Marinković, S. Jovanovic, Gamma-Ray-Induced Structural Transformation of GQDs towards the Improvement of Their Optical Properties, Monitoring of Selected Toxic Compounds, and Photo-Induced Effects on Bacterial Strains, 12 (2022) 2714. https://doi.org/10.3390/nano12152714.

[72] C. Zhao, X. Li, C. Cheng, Y. Yang, Green and microwave-assisted synthesis of carbon dots and application for visual detection of cobalt(II) ions and pH sensing, Microchemical Journal, 147 (2019) 183-190. https://doi.org/10.1016/j.microc.2019.03.029.
[73] R.-X. Zhao, A.-Y. Liu, Q.-L. Wen, B.-C. Wu, J. Wang, Y.-L. Hu, Z.-F. Pu, J. Ling, Q. Cao, Glutathione stabilized green-emission gold nanoclusters for selective detection of cobalt ion, Spectrochimica Acta Part A: Molecular and Biomolecular Spectroscopy, 254 (2021) 119628. https://doi.org/10.1016/j.saa.2021.119628.
[74] Y. Vasseghian, E.-N. Dragoi, F. Almomani, N. Golzadeh, D.-V.N. Vo, A global systematic review of the concentrations of Malathion in water matrices: Meta-analysis, and probabilistic risk assessment, Chemosphere, 291 (2022) 132789. https://doi.org/10.1016/j.chemosphere.2021.132789.
[75] M. Wang, K. Su, J. Cao, Y. She, A.M. Abd El-Aty, A. Hacımüftüoğlu, J. Wang, M. Yan, S. Hong, S. Lao, Y. Wang, "Off-On" non-enzymatic sensor for malathion detection based on fluorescence resonance energy transfer between β-cyclodextrin@Ag and fluorescent probe, Talanta, 192 (2019) 295-300. https://doi.org/10.1016/j.talanta.2018.09.060.
[76] Q. Chen, R. Sheng, P. Wang, Q. Ouyang, A. Wang, S. Ali, M. Zareef, M.M. Hassan, Ultra-sensitive detection of malathion residues using FRET-based upconversion fluorescence sensor in food, Spectrochimica Acta Part A: Molecular and Biomolecular Spectroscopy, 241 (2020) 118654. https://doi.org/10.1016/j.saa.2020.118654.

Table 1. Elementar analysis of p-GQDs, GQDs-25-EDA, and GQDs-50-EDA.

Sample	**N** (wt.%)	**C** (wt.%)	**H** (wt.%)	**S** (wt.%)
p-GQDs	/	44.32	5.27	/
GQDs-25-EDA	7.42	53.24	7.14	/
GQDs-50-EDA	6.81	54.47	7.21	/

Table 2. Results obtained using different types of optical probes for Fe^{3+} based on fluorescence quenching.

Type of fluorescent Probe	**Limit of detection ($\mu molL^{-1}$)**	**Linear range ($\mu mol\ L^{-1}$)**	**Mechanism**
CQDs [55]	3.70	0-20	turn-off
GQDs [56]	2.50	0-50	turn-off
N-GQDs [57]	2.37	1600-10000	turn-off
N-GQDs [54]	1.49	0-300	turn-off/turn-on probe for Fe^{3+} and ascorbic acid
GQDs-25-EDA (presented work)	2.55	0-45	turn-off

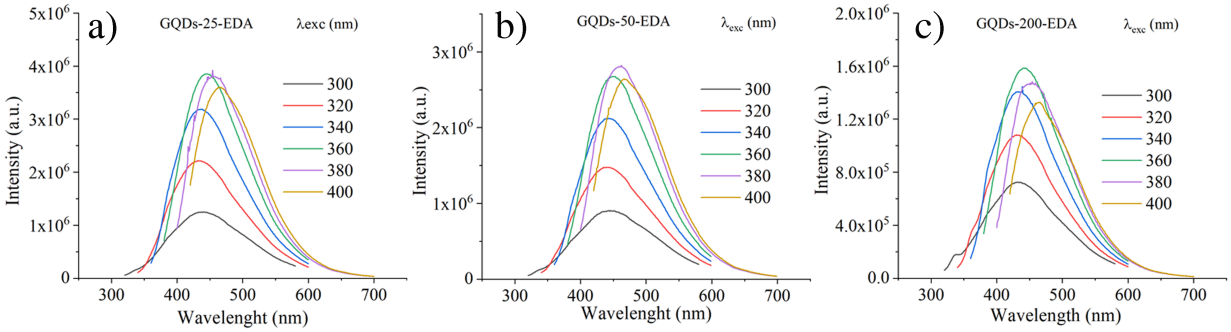

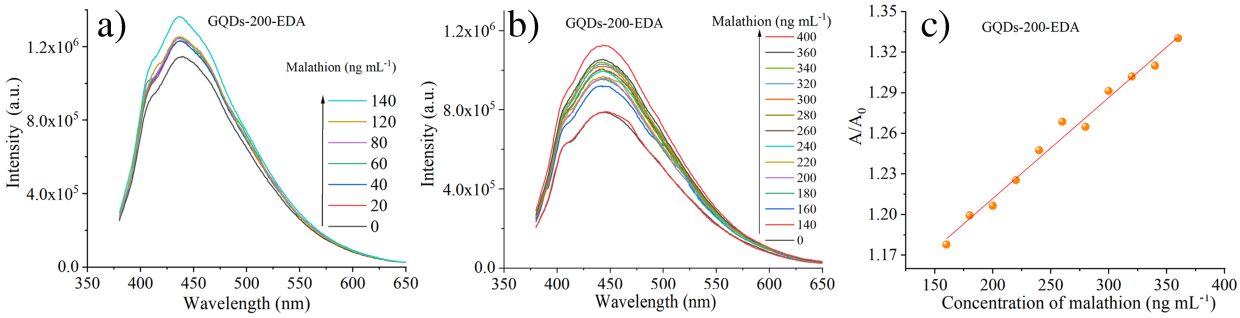

- Amino GQDs were tested as PL sensors for Co^{2+}, Pd^{2+}, Fe^{3+} and Malathion
- PL intensity of GQDs was quenched with Co^{2+}, Pd^{2+} and Fe^{3+} ions
- For the first time, Pd^{2+} were detected by GQDs with LOD 657 nmol L^{-1}
- Malathion enhance PL intensity and LOD was 94 nmol L^{-1}
- GQDs are characterized as non-cytotoxic material

Declaration of interests

☑ The authors declare that they have no known competing financial interests or personal relationships that could have appeared to influence the work reported in this paper.

☐The authors declare the following financial interests/personal relationships which may be considered as potential competing interests: